2017

BMI, Tumor Lesion and Probability of Femur Fracture: a Probabilistic Biomechanics Approach

zhi gao
University of Massachusetts Amherst

BMI, Tumor Lesion and Probability of Femur Fracture: a Probabilistic Biomechanics Approach

A Thesis Presented

by

ZHI GAO

Submitted to Graduate School of the
University of Massachusetts Amherst in partial fulfillment
of the requirements for the degree of

MASTER OF SCIENCE IN MECHANICAL ENGINEERING

September 2017

Mechanical &Industrial Engineering

BMI, Tumor Lesion and Probability of Femur Fracture: a Probabilistic Biomechanics Approach

A Thesis Presented

by

ZHI GAO

Approved as to style and content by:

Ian R. Grosse, Chair

Maureen Lynch, member

Frank Sup, member

Sundar Krishnamurty, Department Head
Mechanical & Industrial Engineering

ACKNOWLEDGEMENTS

I would thank my advisor Professor Ian R. Grosse, for his patient guidance throughout my pursuit of master's degree. He introduced me into the field of biomechanics and stimulated my academic interest in solving existent problems with various approaches. Also, he gave me a lot of help demonstrating the way of good writing and corrected my grammatical errors many times.

ABSTRACT

BMI, TUMOR LESION AND PROBABILITY OF FEMUR FRACTURE: A PROBABILISTIC BIOMECHANICS APPROACH

SEPTEMBER 2017

ZHI GAO

B.S., CHINA UNIVERSITY OF MINING AND TECHNOLOGY

M.S.M.E., UNIVERSITY OF MASSACHUSETTS AMHERST

Directed by: Professor Ian R. Grosse

Sideways falls are the major cause of hip fractures for elder people and many researches have been done to explore the influence of possible factors. In reviewing previous studies and health investigations, we have found that most of these factors are directly or indirectly linked to subjects' BMI (body mass index). Thus, from a statistical perspective, BMI could be an overall indicator of the probability of femur fracture from a sideways fall. Using a biomechanics approach coupled with statistical data we investigate this relationship with a large cohort of postmenopausal women aged 50-79 from WHI-OS (Women's Health Initiative Observational Cohort). The cohort is divided into six sub-cohorts by BMI where each fall-related factor is examined and compared with each other. Significant differences are discovered among cohorts in terms of femur size, aBMD (areal bone mineral density), peak fall force based on kinematics, and maximum von Mises stresses induced in the proximal femur. Through a probabilistic margin of safety approach which has been recently applied to orthopedic application, we found the margin of safety predicted probability to be decreasing faster with increasing BMI and better

fitted with medical record of the identical cohort compared to that found using a deterministic risk factor approach. To promote the application in other situations, tumor damaged femur bones are examined and tested for possible stress concentration effect in terms of probability of failure. The influence of tumor lesion turned out to be size and location sensitive. The superior side of the femoral neck has the highest stress concentration effect from tumor lesion where a 4mm diameter lesion could result in a 1.7 times greater maximum von Mises stress and 2.95 times greater probability of failure.

TABLE OF CONTENTS

LIST OF TABLES

LIST OF FIGURES

CHAPTER 1

INTRODUCTION

1.1 Research Overview

Hip fractures due to sideways falls are serious problems among elder people, especially postmenopausal women since bone mineral content is reduced(W. C. Hayes et al., 1993), (Grisso et al., 1991), (Cummings et al., 1995). Many organizations like health care centers, clinics and hospitals have sought to establish statistical links between probability of hip fall fracture and medical observations such as medical care histories, life styles, demographics, etc.(Beck et al., 2009), (Cauley et al., 2010)(Nielson et al., 2011).

Insights of fall biomechanics were obtained by reproducing falls with controlled variables from either volunteers with protections (van den Kroonenberg, Aya J, Hayes, & McMahon, 1996) or surrogate pelvis release experiments with sensors recording dynamic parameters(Robinovitch, McMahon, & Hayes, 1995). (W. Hayes & McMahon, 1991) adopted force plate with pelvis release experiment to develop the mass-spring-damper model and explored the stiffness of pelvis and effective mass of male and female subjects respectively.

Then finite element analysis (FEA) was introduced in the field to obtain the stress/strain conditions within the bone, which is also a good reference for the load to strength ratio/factor of risk(Orwoll et al., 2009)(Amin et al., 2011). (Dragomir-Daescu et al., 2011) compared FEA results and femur mechanical tests, validating the elasticity with respect to bone mineral density (BMD) as well as the yield criterion. Easley et

al.(Easley et al., 2007) introduced FE-based probabilistic approach to orthopedic biomechanics and investigated random variables in hip stem model and total knee replacement as sensitivity factors.

The objective of this research is to apply FE based probabilistic approach to quantify the relationship of BMI to the probability of proximal femur fracture from a sideways hip fall. As part of this process we account for various uncertainties and randomness of important factors known to be correlated to BMI and which affect the biomechanics of bone fracture from a fall. (Beck et al., 2009) investigated a large postmenopausal women cohort and discussed the correlation between obesity and physical conditions of proximal femurs by BMI category. From both deterministic approach and probabilistic approach, we reviewed such correlation and compared the results with each other.

Following previous hip fall experiments and simulations, the peak fall force on hip served as both predictor of fracture risk and input parameter for von Mises stress. The stress result considered not only the force but also the femur geometry and material properties and thus is considered more comprehensive.

Then we introduced the probabilistic approach coupled with FEA method in a manner similar to the work of Easley et al.(Easley et al., 2007) where the parameters were treated as random variables. Those from direct observation such as subjects' physical conditions were treated as independent random variables while others served as dependent random variables which were transferred from existing random variables using the transition functions. The probabilistic FEA tool enabled the probability density functions (pdfs) associated with maximum von Mises stress based on the conditions for each BMI cohort respectively. This coupled with probability density functions for bone strength enabled

failure probabilities to be computed, and the results were compared with medical records of hip fracture incidence rate from the same literature.

However, these conclusions and findings are aimed to healthy patients with intact femur bones. There could be bone damages prior to the sideways falls, such as bone tumor which consumes healthy bone tissue and undermines the structural strength. Previous studies used CT scan to obtain geometry information of tumor lesions and the dimension of the lesion was then put into an empirical formula based on clinical cases review to estimate failure probability. The formula is a ratio between calculated rigidities from lesion infected bone and healthy bone which could be the contralateral limb or corresponding limb from another individual in a similar condition to keep accuracy of estimation(Snyder et al., 2006).

1.2 Research scope

The goal of this research is to introduce the probabilistic approach coupled with finite element method to predict the probability of a fracture in a sideways fall under the influence of BMI(body mass index) and tumor damage. The probabilistic margin of safety approach as reliability assessment in engineering was recently introduced into the biomechanics field by (Easley et al., 2007) as a tool of sensitivity analysis in orthopedic application. As for sideways fall analysis and prevention, the probabilistic approach coupled with finite element analysis is able to include the distributions of different factors and conduct the probability of failure as a result. Therefore, the physical conditions of subjects in this study are treated as random variables and converted via transition functions to yield the falling conditions which are also random variables. With the

probabilistic tool we obtain the von Mises stress as random variables and evaluate the probability of failure by comparison with the bone strength.

In reviewing a specific cohort from statistics level(Beck et al., 2009), we found that BMI affects many important factors, including peak fall force, femur geometry, BMD (bone mineral density) and mechanical property. All the factors come together to affect the stress and probability of failure to a great extent, indicating that the BMI could be a comprehensive indicator for femur fracture in a sideways fall.

Taking a step further that the influence of bone tumor can be estimated with proper simplification and parameterization based on the cohort information obtained from above. Tumor lesions are idealized as spherical cavity in bone with center point through the surface of the cortical bone shell of the proximal femur. Diameter and anatomical site defines the tumor condition as parameters and probability of failure is obtained within each BMI cohort.

1.3 Thesis outline

There are eight chapters in this thesis. Chapter 1 is the introduction of the thesis, presenting the motivation and scope for the study. The background information in Chapter 2 introduces the target field to be studied including sideways fall and bone tumor as well as the method which is finite element analysis. Chapter 3 presents the model of femur and the boundary conditions, namely the peak fall force and the way how femur is constrained in a simulated sideways fall. Chapter 4 presents the cohort information including the physical conditions of the subjects and DXA(dual X-ray absorption) results of the femur bones. Chapter 5 introduces the probabilistic approach and how it is coupled with finite element analysis. Chapter 6 presents the result of healthy bones under the

influence of BMI and validate the probabilistic approach with medical records. Chapter 7 presents the results of tumor damaged femur bone in a sideways fall based on the stress concentration factors and the probabilistic approach. Chapter 8 discusses the findings and the future works to be done.

CHAPTER 2

BACKGROUND

2.1 FEA (finite element analysis)

The finite element analysis is a numerical method to find approximate solutions for boundary value problems. Back in the 1940s, the need for solving complex civil and aerodynamics problems drove the early appearance of finite element method. In the 1956 the paper by Turner, Clough, Martin and Topp introduced a new method dividing structures into elements to solve for plane stress and it was recognized as the start of finite element method(Turner, Clough, Martin, & Topp, 1956). In 1960 Clough first proposed the word of "finite element" in the paper "the finite element in plane stress analysis". O. C. Zienkiewicz realized the general application of FEA and firstly presented the subject in his book of <The Finite Element Method> (Zienkiewicz, Taylor, Zienkiewicz, & Taylor, 1977) which is most recognized textbook in the field. With a lot of mathematicians' work in this period people realized the displacement model is a form of Rayleigh-Ritz method and more mathematical models for different fields were proposed (Felippa, 2004). The publication of <An Analysis of The Finite Element Method> in 1973 by Strang and Fix has provided robust mathematical foundation. As the rapid growth of the computer technology, the application of finite element method was also greatly expanded. Large finite element method software companies such as ANSYS, ADINA, ABAQUS are used in many fields these days, including the solid mechanics, magnetic flux field, fluid dynamics and heat conduction problems.

The application of FEA in the medical field helps understand the stresses in tissues such as muscles, blood vessels and bones. Rather than hiring volunteers wearing sensors to simulate certain activities, FEA is able to obtain the real-time information about the strains and stresses in 3D. Some of the dangerous experiments that cannot be complied by volunteers due to ethic reasons can be analyzed in simulations under destructive conditions with the help of FEA.

2.2 Sideways Fall and Hip Fracture

Accidental falls are common and serious problems among the elderly due to medical treatments, poor vision and balance problems(Abdelhafiz & Austin, 2003)(Felson et al., 1989)(Ray, Griffin, Schaffner, Baugh, & Melton III, 1987)(Greenspan, Myers, Maitland, Resnick, & Hayes, 1994) which might cause multiple injuries including cuts, bruises, broken bones, head trauma, fractured hips, and neck and back problems. Hip fractures, which mostly caused by sideways falling(W. C. Hayes et al., 1993), are serious injuries requiring surgical treats and long-term physical therapy afterwards(Magaziner et al., 2000).

Each year, 2.8 million older people are treated in emergency departments for fall injuries. Over 800,000 patients a year are hospitalized because of a fall injury, mostly because of a head injury or hip fracture(a Fall, What Can Happen After,).

2.3 Bone Tumor

A bone tumor is a lump of abnormal tissue as a result of uncontrolled bone cell growth. When the bone tumor originates in the bone, it is classified as “primary tumors” which could be “benign” or “cancerous”. When the tumor cell travels from other cancerous tissue like breast cancer, lung cancer or prostate cancer, it is classified as secondary

tumor, also known as metastatic tumor. The common types of bone tumor are: Osteosarcoma, Ewing's sarcoma, chondrosarcoma, spindle cell sarcoma(AAOS.org,).

From the mechanical aspects, the uncontrolled growth of bone tumors deals damage to surrounding healthy tissues and weakens the bone, some of which causes pathologic fractures to bone themselves. For example, Figure 0.1 shows the tumor dealing severe damage to femur bone, resulting in a pathologic fracture(pathorama.ch, 2017).

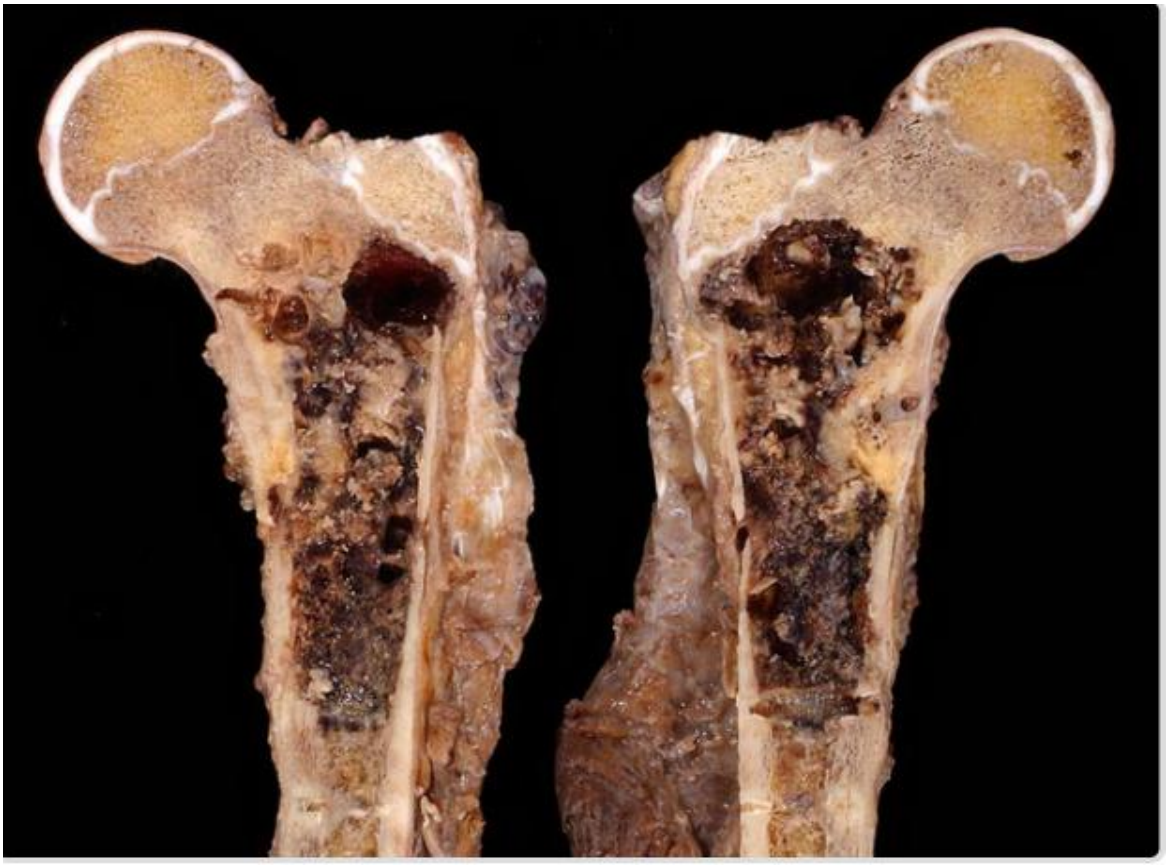

Figure 0.1 Telangiectatic osteosarcoma involving the femur in an 11 y/o male(pathorama.ch, 2017)(auto-permitted for educational purpose only by Pathorama).

The radio graph (Snyder et al., 2006) in Figure 0.2 shows the bone tumor in the proximal femur, growing and destructing the femur bone structure from inside. The outer cortical shell of proximal femur is noticeably weakened and becomes irregular and thinner than normal.

Figure 0.2 Anteroposterior and lateral radiographs of a fracture through a unicameral bone cyst at the base of the proximal(Snyder et al., 2006)(used with permission).

From the examples above, the influence of tumors is significant and predictable in clinics with radio graphs. The probability of a hip fracture in a sideways fall under the influence of bone tumor should be evaluated as a reference for related patients.

CHAPTER 3

MODEL AND BOUNDARY CONDITIONS

3.1 Femur Model

The femur bone model was obtained from GrabCAD® by the author of Negar An, which is one of the mostly user-adopted femur models in the category that also recognizes the cortical bone and trabecular bone. In the author's response, it is a left femur bone from a cadaver, but no further information about the gender, race or age was revealed. However, an important goal of this research is to establish a method for determining the direct influence of BMI and tumor lesions on the probability of femur fracture from a sideways fall. Accounting for individual morphological differences in the femur other than general isometric size changes in femur morphology is beyond the scope of this study.

The original femur model and cross-sectional views are shown in Figure 0.1.

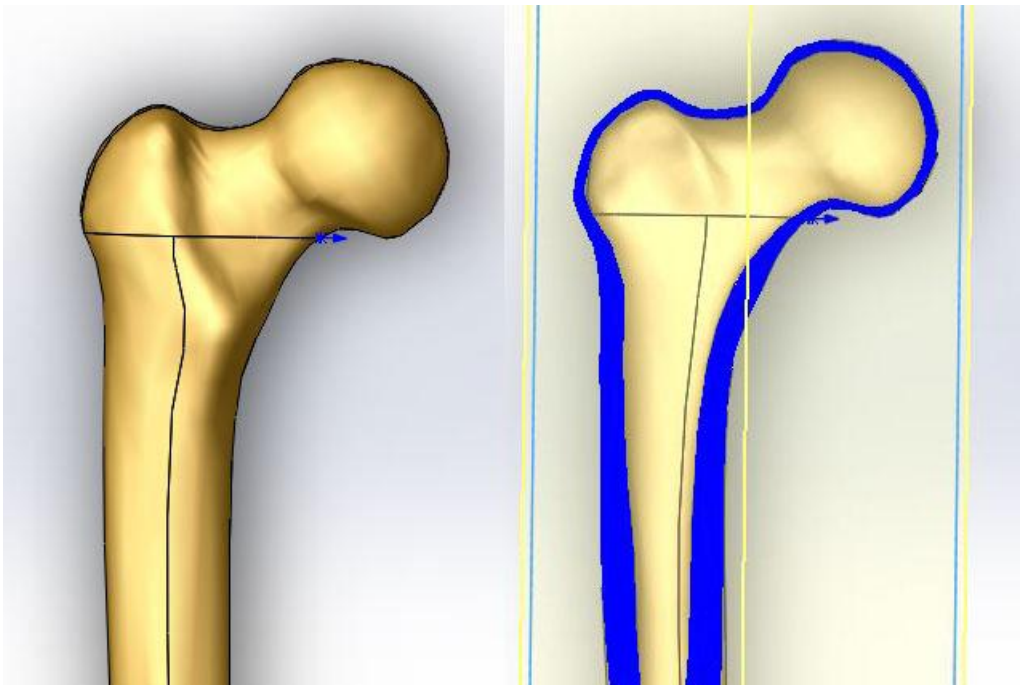

Figure 0.1 Originate femur model from Negar An and the intersection view.

However, the cortical bone shell of proximal femur is found to be too thick after careful comparison with existing femoral QCT scans according to the Fig. 4 from Julio Carballido-Gamio et al.(Carballido-Gamio et al., 2015).

The model is modified in Solidworks (Dassault Systèmes SolidWorks Corp) with the reference of the scan results of (Carballido-Gamio et al., 2015). To modify the cortical bone shell with irregular geometry, a series of parallel planes are created to capture the profiles of cross-section which is illustrated in Figure 0.2.

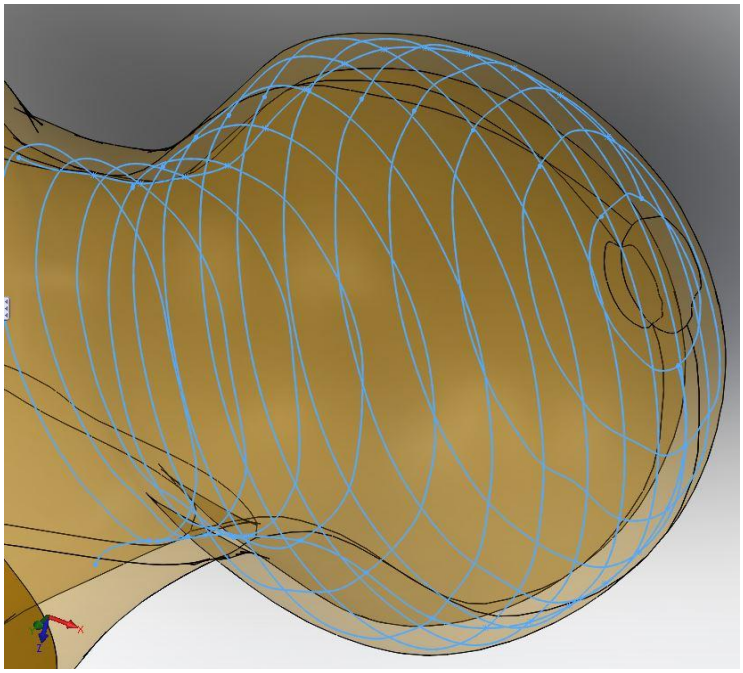

Figure 0.2 Planes created to obtain the intersection lines with the model.

Upon each plane, the intersection curve of outer surface of proximal femur bone is to be offset for a given distance as the new surface's intersection curve. In Figure 0.3, the yellow dotted curve marks the distance with the outer surface intersection curve where the distance is referred to literature of QCT scans.

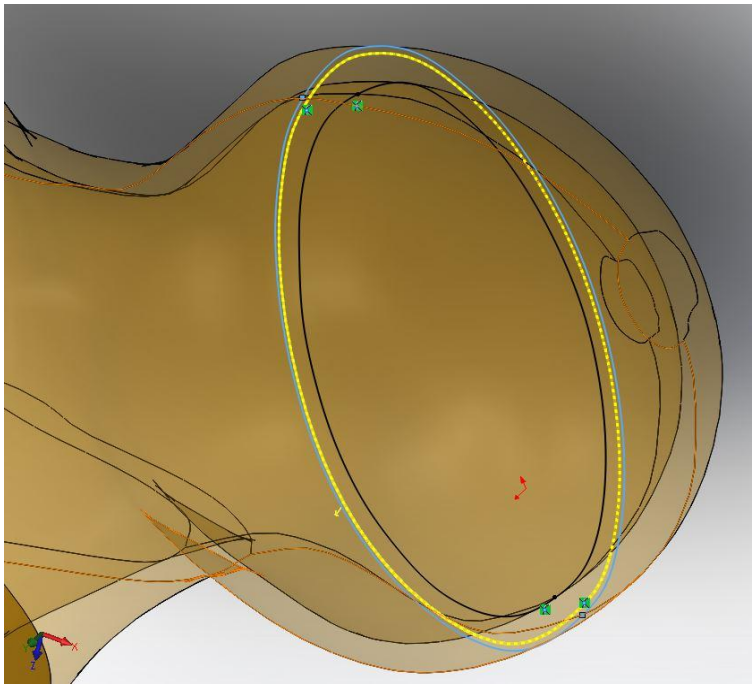

Figure 0.3 Offset of the intersection line.

Based on all the modified intersection lines, a new inner surface is interpolated in Figure 0.4 which also modifies the original cortical bone material with the loft cut function in Solidworks (Dassault Systèmes SolidWorks Corp). Any cortical bone material from original model that coincides with the loft-cut inner surface will be deleted through a minus Boolean operation.

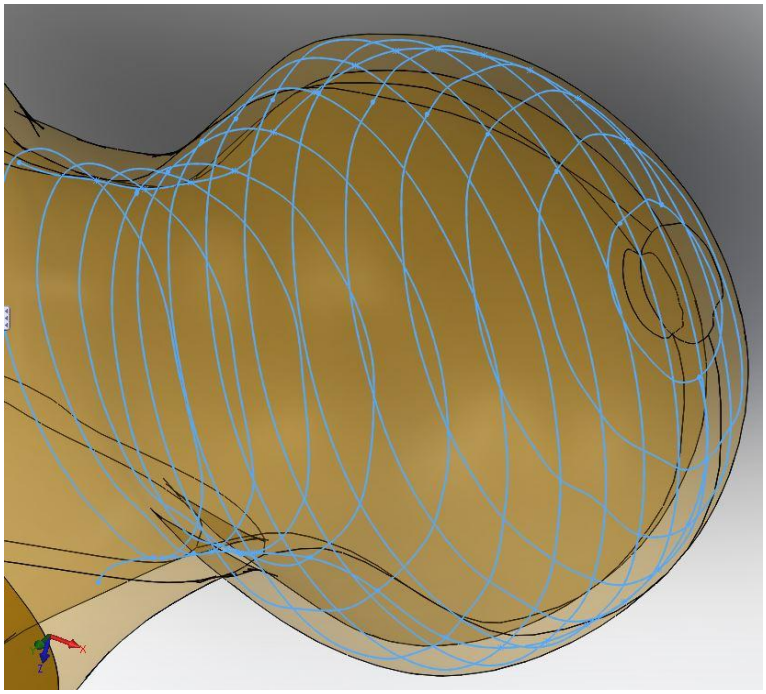

Figure 0.4 Modified intersection lines of the inner surface.

The anterior-posterior intersection view of the modified model is presented in Figure 0.5 which is also agreed with the intersectional view of (Dragomir-Daescu et al., 2011).

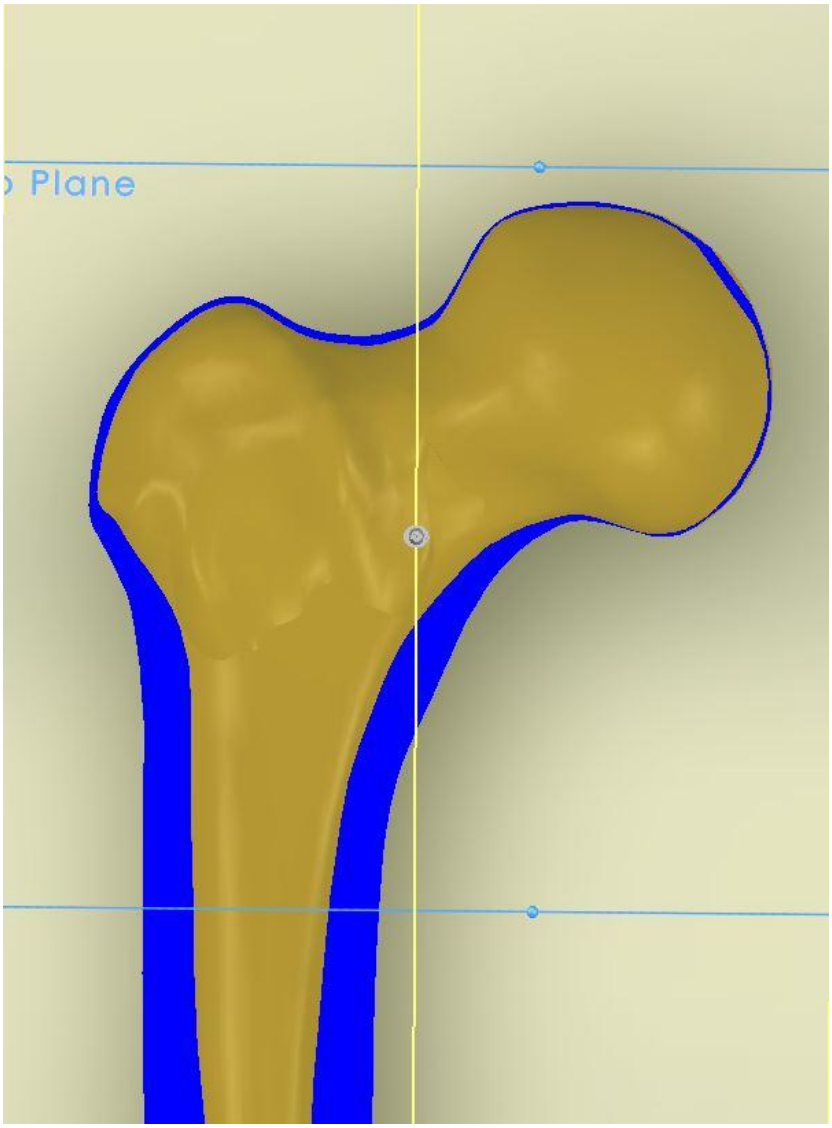

Figure 0.5 cross-sectional view of after-modification femur model.

The thickness analysis is also performed to examine the quality of the modification in Figure 0.6.

Note that the apex of femoral head which is the start point of the modification has a higher thickness than surrounding structures. However, such abnormal region is believed

to have little influence to the result since its location is within the force-applying area as part of the boundary conditions.

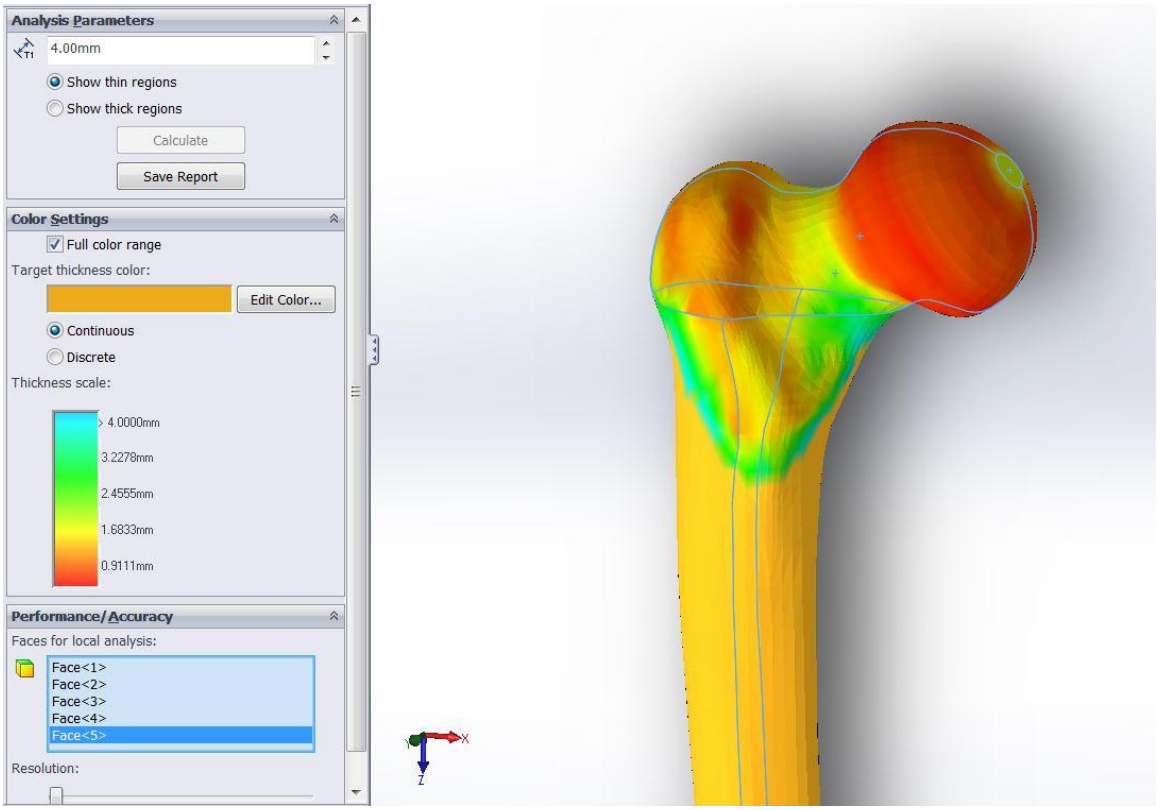

Figure 0.6 Thickness measurement in SolidWorks after modification.

The trabecular bone is then created within the cortical bone as an isotropic solid under a Boolean operation. The distal part of femur is truncated as previous studies for computational efficiency(Zysset et al., 2015)(Nishiyama, Gilchrist, Guy, Cripton, & Boyd, 2013)(Dragomir-Daescu et al., 2011).

3.2 Load Conditions

The femur model is placed 10 degrees to horizontal plane to simulate the inverse angle of human femur in a sideways fall(Dragomir-Daescu et al., 2011). The impact force is applied to a circular region on femoral head while fixed support is placed on the greater trochanter as illustrated in Figure 0.7.

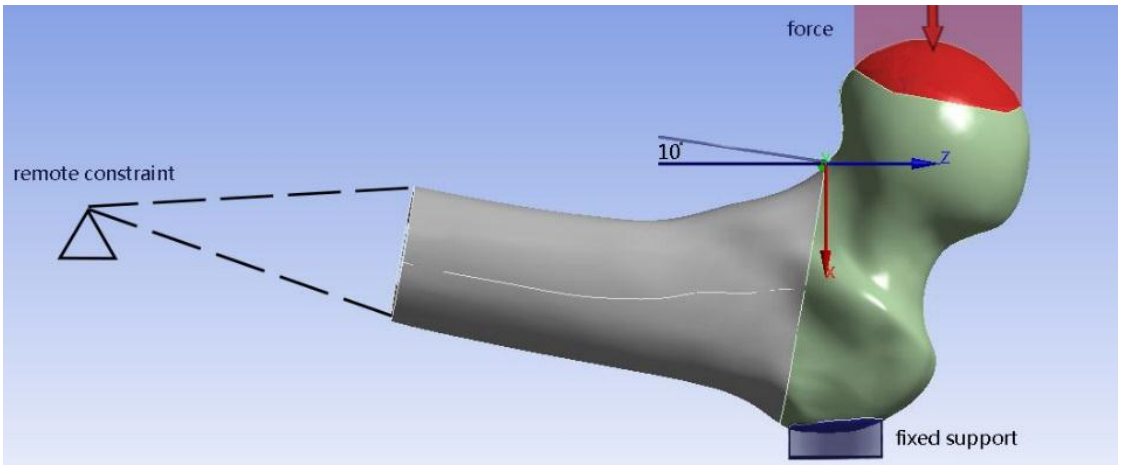

Figure 0.7 illustration of load and supports.

3.3 Peak Fall Force

The peak force experienced by the hip during a sideways fall can be estimated through a kinematics approach(W. Hayes & McMahon, 1991)(Bouxsein et al., 2007). The potential energy from standing high to the ground is

$$E = m_{eff} g h_{eff} \quad (1)$$

where g is acceleration constant of gravity which is taken as 9.8m/s^2, h is effective height when sideways fall happens taken as 0.5 times of an individual's total height (m), m is the effective mass (Kg). According to Hayes et al., the subjects' arms and lower limbs might touch the ground before the body trunk in a fall, but this does not reduce the downward velocity of hip. Instead, this "initial contact" reduces effective body weight (moving mass) which is approximately half of the total weight among female participants in practice(W. Hayes & McMahon, 1991).

When the hip initially contacts the ground, the downward velocity of it reaches the maximum value and all of the potential energy converts into kinematic energy. Afterwards the velocity is reduced while the soft tissue is compressed, giving more support to the femur bone. When the downward velocity is zero, the falling halts,

meaning all kinematic energy is converted to elastic energy. Now we observe the force at its maximum value.

$$E = \frac{1}{2}Kx^2 = \frac{1}{2}\frac{F^2}{K} \tag{2}$$

The stiffness of floor is referred to "firm" type floor with a stiffness of 263 kN/m from Laing et al. (Laing, Tootoonchi, Hulme, & Robinovitch, 2006) in this study. The hip stiffness K_{hip} (kN/m) based on soft tissue thickness t (mm) is obtained by regression analysis (R^2=0.8401) by Robinovitch et al.(W. Hayes & McMahon, 1991)

$$K_{hip} = 625.6 \cdot t^{-0.9009} \tag{3}$$

Considering the ground or floor on which people might fall has a certain value of stiffness, the K should be the total stiffness of the hip soft tissue and the ground in series as calculated:

$$K_{total} = \frac{K_{hip} \cdot K_{floor}}{K_{hip} + K_{floor}} \tag{4}$$

Where t refers the thickness of soft tissue thickness in units of mm. In addition, Maitland, L. A. et al. demonstrated BMI is a good predictor for trochanteric soft tissue thickness(Maitland, Myers, Hipp, Hayes, & Greenspan, 1993). Dufour et al. (Dufour et al., 2012) has conducted the formula between thickness t and BMI for both genders, allowing us to obtain total hip-floor stiffness based on BMI data of target cohorts.

Considering Eqn. (1), (2) and (4) yields

$$F_{peak} = \sqrt{2 \cdot g \cdot h_{eff} \cdot m_{eff} \cdot K_{total}} \tag{5}$$

3.4 The von Mises stress yield criterion

The von Mises stress, also named as equivalent stress, is used in this study for bone fracture criterion. At any point of the femur bone, the von Mises stress is calculated as

$$\sigma_{vm} = \sqrt{\frac{1}{2}\left[(\sigma_1 - \sigma_2)^2 + (\sigma_2 - \sigma_3)^2 + (\sigma_3 - \sigma_1)^2\right]} \quad (6)$$

where σ_1, σ_2 and σ_3 are the principal stresses. The von Mises stress is obtained through the sideways fall simulations and the maximum von Mises stress is marked for the comparison with the bone strength which is referred to uniaxial mechanical test and bone mineral density.

The von Mises stress, as well as the peak fall force is taken as a direct indicator for the risk of bone fractures. Probability of failure is calculated based on the maximum von Mises stress state which is also compared with the medical records from the identical cohorts for validation and discussion.

CHAPTER 4

TARGET COHORT

4.1 A study of the postmenopausal women subjects

Beck et al. had a research about the WHI(Women's Health Initiative) which is one of the largest long-term health studies to find out whether the obesity can make the femur stronger among postmenopausal women. These aged female subjects are also high-risk cohorts to sideways fall injuries and women subjects are even susceptible due to the bone mass lost from menopause(Beck et al., 2009).

The cohort was divided by subjects' BMI which is the ratio between the body mass and the square of the body height to describe the degree of obesity. Six BMI cohorts were established which are underweight(<18.5), healthy weight(18.5-25), overweight (25-30), mild obesity(30-35), moderate obesity(35-40) and extreme obesity(>40). The information of each cohort is present in Table 0.1.

Table 0.1 Body information about the target cohort from Beck et al.

	BMI categories					
	Underweight ≤18.5	Healthy weight 18.5~25	Overweight 25~30	Mild Obesity 30~35	Moderate Obesity 35~40	Extreme Obesity ≥40
subjects	205	1744	1601	688	243	161
mass(Kg)	46.3±4.7	59.5±6	71.4±6.2	83.4±7.2	97.2±9.1	111.1±11.7
height(m)	1.626±0.06	1.624±0.06	1.617±0.06	1.611±0.06	1.614±0.06	1.597±0.09
BMI	17.51±2.27	22.56±2.85	27.30±3.14	32.13±3.66	37.31±4.68	43.56±6.84
Age(yr)	65.4±6.9	64.3±7.3	64.2±7.3	64.48±7.2	62.3±7.1	61.2±7.1

As seen in the table, majority of the subjects are within the healthy and overweight categories which together takes 72.1% of the total number. The height and age of these subjects does not have a clear trend of variation with respect to the BMI.

To correctly estimate the peak fall force of the subjects, the trochanteric soft tissue thickness is required based on the cohort information. The correlation between BMI and trochanteric soft tissue thickness for women subjects according to Dufour et al.(Dufour et al., 2012) is

$$t = 2.3415 \cdot BMI - 33.444 \tag{7}$$

The trochanteric soft tissue thickness t is correlated to BMI while the hip stiffness K is correlated to t, providing the approach for the total stiffness K_{total} of the peak fall force calculation. The intermediate variables for calculating the force are shown in Table 0.2.

Table 0.2 The calculation of peak fall force

	BMI categories					
	Underweight	**Healthy weight**	**Overweight**	**Mild Obesity**	**Moderate Obesity**	**Extreme Obesity**
	≤18.5	**18.5~25**	**25~30**	**30~35**	**35~40**	**≥40**
BMI(kg/mm^2)	**17.51 ±2.27**	**22.56 ±2.85**	**27.30 ±3.14**	**32.13 ±3.66**	**37.31 ±4.68**	**43.56 ±6.84**
Soft tissue thickness(mm)	**7.56 ±5.3**	**19.38 ±6.7**	**30.49 ±7.4**	**41.79 ±8.6**	**53.93 ±11.0**	**68.55 ±16.0**
K of pelvis(kN/m)	**102.06 ±3.13**	**43.50 ±3.13**	**28.85 ±3.13**	**21.68 ±3.13**	**17.21 ±3.13**	**13.85 ±3.13**
Total K(kN/m)	**73.548 ±1.699**	**37.326 ±1.751**	**25.998 ±1.761**	**20.029 ±1.764**	**16.153 ±1.766**	**13.157 ±1.767**
Peak Fall Force(N)	**5207.7 ±305.5**	**4203.6 ±287.2**	**3834.4 ±293.8**	**3630.4 ±331.4**	**3523.3 ±386.5**	**3381.2 ±451.2**

4.2 Cortical Bone Material properties

Subjects of (Beck et al., 2009) were scanned with DXA(duel X-ray absorption) on the hip and arranged by the BMI. The DXA scan locations of the mineral mass profiles are shown in Figure 0.1.

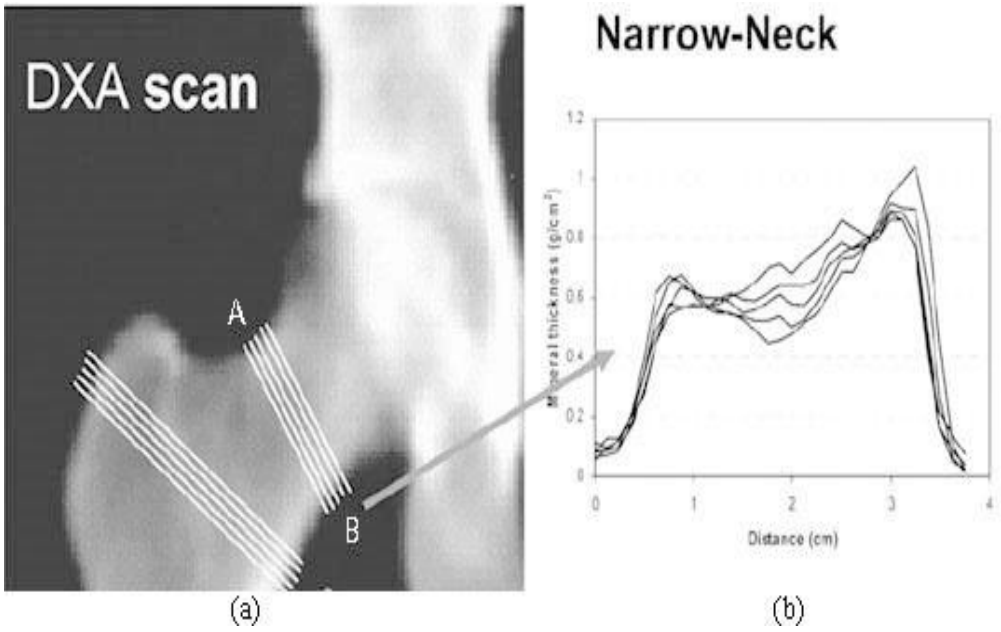

Figure 0.1 the DXA scan of proximal femur from Beck et al.(Beck et al., 2009)(used with permission).

However, the DXA scan only gives areal bone mineral density as scan result because the DXA divides the bone mineral content by the projection area to get aBMD that ignores the third dimension which is the depth in terms of the projection plane. In Figure 0.1(a) each white line marks a scan profile of mineral mass and each location contains five profiles. Corresponding mineral mass profiles are reflected in Figure 0.1(b) where the averaged data is collected in Table 0.3. The outer diameter of narrow neck D is the length of the white lines and the distance between two adjacent lines is the width of a single scan.

In addition, (Beck et al., 2009) adopted the HSA (hip structure analysis) method to extract more geometry information such as cross-sectional area and section modulus from the sites of narrow neck, intertrochanter and mid shaft of femur. It is able to calculate for the volumetric BMD information with the help of cross-sectional area information of corresponding anatomic sites. However, such variation on BMD among different sites

within a single femur are ignored in this large scale investigation for the purpose of convenience and simplicity. Instead, the BMD of narrow neck is selected for a sideways hip fall. Differences among individuals are reflected as BMD distributions of the BMI cohort. The DXA and HSA results for different BMI cohorts are reported in Table 0.3.

Table 0.3 DXA and HSA scan results from Beck et al.(Beck et al., 2009)

	BMI categories					
	Underweight	**Healthy weight**	**Overweight**	**Mild Obesity**	**Moderate Obesity**	**Extreme Obesity**
	≤18.5	**18.5~25**	**25~30**	**30~35**	**35~40**	**≥40**
Femoral neck aBMD(g/cm2)	**0.616 ±0.114**	**0.663 ±0.083**	**0.708 ±0.080**	**0.739 ±0.104**	**0.786 ±0.124**	**0.821 ±0.126**
Femoral neck outer D (mm)	**2.98 ±0.200**	**3.00 ±0.167**	**3.02 ±0.200**	**3.04 ±0.210**	**3.03 ±0.218**	**3.07 ±0.228**
CSA(mm2)	**1.74 ±0.300**	**1.89 ±0.292**	**2.03 ±0.280**	**2.14 ±0.314**	**2.26 ±0.327**	**2.39 ±0.342**
Shaft diameter(mm)	**2.80 ±0.172**	**2.81 ±0.167**	**2.84 ±0.160**	**2.88 ±0.184**	**2.92 ±0.187**	**2.95 ±0.190**

Figure 0.2 shows the principle of DXA scan. The ring-shaped body represents the cortical bone shell of proximal femur and the grey plane represents the projection plane on which the projection area A is calculated. DXA scan divides BMC(bone mineral content) by the A(projection area) to get aBMD in Eqn (8).

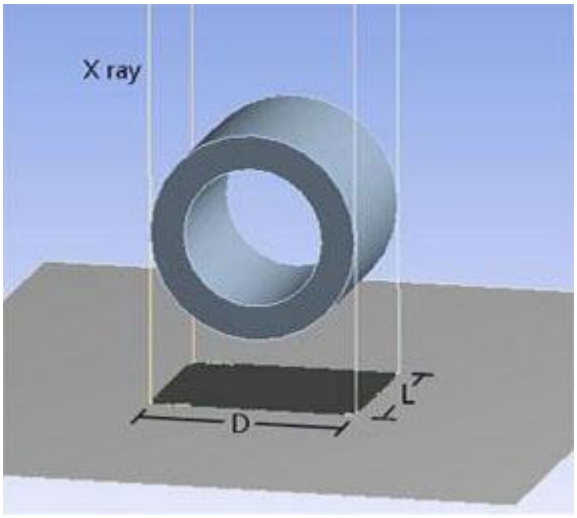

Figure 0.2 Illustration of DXA scan.

$$aBMD = \frac{BMC}{A} \tag{8}$$

where the projection area is

$$A = D \cdot L \tag{9}$$

D (cm) is the outer diameter of the scan region and is also the length of white lines in Figure 0.1(a). L is unit length of the scan and will cancel out itself in the conversion. With the CSA(cross-section area) provided in HSA, the volumetric BMD is obtained as

$$vBMD_{cort} = \frac{BMC}{CSA \cdot L} \tag{10}$$

The specific values of BMC and L are unknown, but they are intrinsic properties for a given part of bone. Thus, substituting Eqn. (8) and Eqn. (9) into Eqn. (10) yields the volumetric BMD with known variables in Eqn.(11).

$$vBMD_{cort} = \frac{aBMD \cdot D}{CSA} \tag{11}$$

Despite there is variation of the BMD within an individual's femur, our interest in this study is variability among individuals across BMI category. That we assumed homogeneity of mechanical and physical properties in both cortical and trabecular bone. The overall averaged BMD for the proximal femur is taken as trabecular BMD according to each of the BMI cohort's femur model with its own total volume V and total projection area PA presented in Figure 0.4. The conversion is shown in Eqn. (12) as

$$vBMD_{trab} = \frac{aBMD_{neck} \cdot PA}{V} \tag{12}$$

The correlation of the elastic moduli of cortical and trabecular bone material to vBMD are obtained from the uniaxial mechanical tests to femoral neck region's samples of 23

donors(Morgan, Bayraktar, & Keaveny, 2003), which was adopted and verified by(Dragomir-Daescu et al., 2011)

$$E = 6.850 \cdot vBMD^{1.49} \tag{13}$$

The yield strain of bone material was also found by mechanical tests on 18 femur specimens with corresponding FEA simulations(Dragomir-Daescu et al., 2011) which is correlated to vBMD as

$$\varepsilon_y = 0.0039 \cdot vBMD_{cort}^{1.42} \tag{14}$$

In terms of uni-axial state of stress, the yield strength is given by

$$S_y \equiv \sigma_y = E\varepsilon_y \tag{15}$$

Considering a much higher elastic moduli and section modulus of the cortical bone shell, the yielding is considered to have occurred when maximum von Mises stress in cortical bone is equal to or greater than cortical bone strength.

The cortical bone material properties including bone mineral density, Young's modulus, yield strain and yield stress are concluded in Table 0.4.

Table 0.4 Cortical bone material properties.

	BMI categories					
	Underweight	**Healthy weight**	**Overweight**	**Mild Obesity**	**Moderate Obesity**	**Extreme Obesity**
	≤18.5	**18.5~25**	**25~30**	**30~35**	**35~40**	**≥40**
vBMD(g/cm3)	**1.055±0.277**	**1.052±0.218**	**1.053±0.2**	**1.05±0.227**	**1.054±0.239**	**1.055±0.236**
cortical bone E(Gpa)	**7.419±2.903**	**7.392±2.281**	**7.401±2.098**	**7.364±2.368**	**7.406±2.501**	**7.415±2.47**
cortical bone εy	**0.0155±0.00160**	**0.0155±0.000999**	**0.0155±0.000843**	**0.0156±0.00108**	**0.0155±0.00119**	**0.0155±0.00116**
cortical bone σy	**115.036±46.56**	**115.016±36.25**	**115.023±33.20**	**114.99±37.82**	**115.027±39.83**	**115.033±39.27**

4.3 Femur Geometry Variation

According to result of the HSA (Beck et al., 2009), the dimensions of proximal femur such as the outer diameters of femur neck, greater trochanter and mid shaft are expanding simultaneously with respect to BMI. Such increases of diameter are found to be approximately proportional to each other, indicating a quasi-uniform expansion in the cross-sectional area of proximal femur due to BMI increase. Since our model was truncated at the trochanteric region, the anatomic length of the proximal femur is not the value of interest, an overall geometry scaling is to be applied on the model for different BMI cohorts. Table 0.5 shows the outer diameter information of different BMI cohorts.

Table 0.5 Outer diameters of the anatomical locations

	BMI categories					
	Underweight	Healthy weight	Overweight	Mild obesity	Moderate obesity	Extreme obesity
Anatomic sites	**≤18.5**	**18.5~25**	**25~30**	**30~35**	**35~40**	**≥40**
Narrow neck(mm)	**2.98**	**3**	**3.02**	**3.04**	**3.03**	**3.07**
Intertrochanter(mm)	**5.02**	**5.04**	**5.1**	**5.18**	**5.23**	**5.27**
Shaft(mm)	**2.8**	**2.81**	**2.84**	**2.88**	**2.92**	**2.95**

However, the narrow neck and intertrochanter regions are highly irregular and the angle of measurement affects a lot to the result which results in large errors. On the contrary, the shaft diameter has simplest geometry with the least ambiguity in measurement and is selected to set the geometry expansion ratio for models.

The mid-shaft diameter of the original femur model is marked as illustrated in Figure 0.3. Ratios between the original model and target BMI cohorts are used to uniformly expand/shrink the model accordingly in SolidWorks® for different simulations.

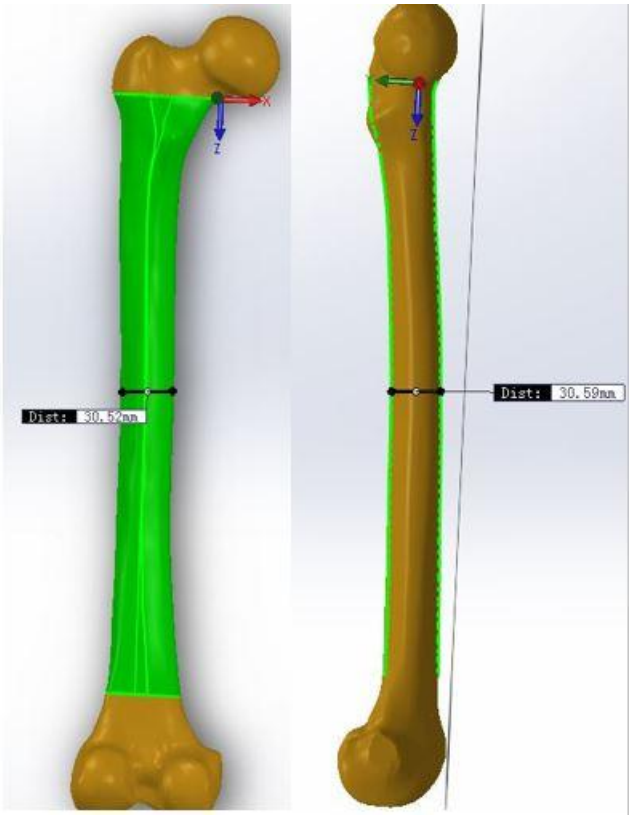

Figure 0.3 The size of the original model.

Here, the pre-select of this program restricted all subjects to be NHW(non-Hispanic white) women which limit the difference of femur shapes to a low level comparing to the interracial differences. Also the difference in specific femur shapes of individuals are averaged by the large quantity of samples and only the femur sizes of different BMI cohorts are clearly revealed in data.

4.4 Trabecular Bone Material Properties

The series of femur models with the same shape but different sizes provide detailed geometry information of different BMI cohorts that allow us to estimate the averaged vBMD out of aBMD. Each BMI cohort's femur model provides a unique anterior-posterior projection area (PA) and volume (V) information with a corresponding aBMD

from Beck et al(Beck et al., 2009). But the change of PA and V among different BMI cohorts are not synchronous because of the dimensions.

As illustrate in Figure 0.4, the BMC is an intrinsic property which stays the same in any type of BMD calculation. The BMC dividing by PA yields an overall averaged BMD and this result is treated as the vBMD for the trabecular bone of the proximal femur since the cortical bone is a thin shell in proximal femur and takes a relatively small portion.

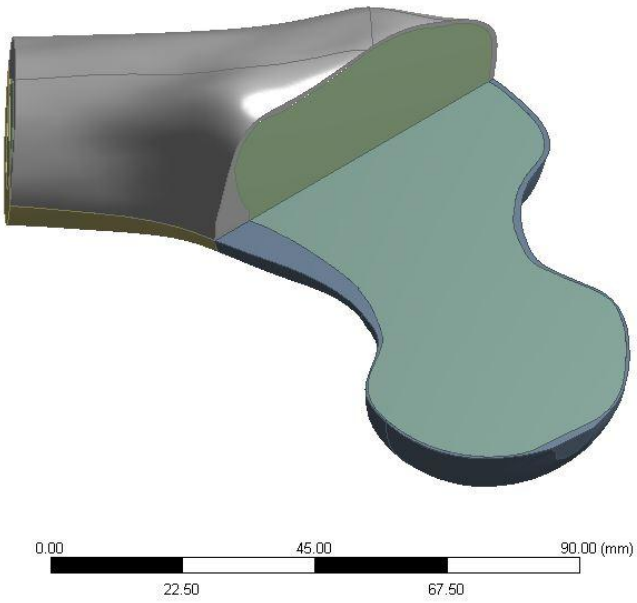

Figure 0.4 cross-sectional view of proximal femur model for PA(projection area) and V(volume).

$$vBMD = \frac{aBMD \cdot PA}{V} \tag{16}$$

Eqn. (17) from Morgan et al.'s observation (Morgan et al., 2003) calculates for the elastic modulus of the trabecular bone in units of MPa.

$$E_{trab} = 8.92 \cdot \left(vBMD_{trab}\right)^{1.83} \tag{17}$$

The trabecular bone's material properties are collected in Table 0.6 for further calculation.

Table 0.6 Trabecular bone material properties.

	BMI Categories					
	Underweight	**Healthy weight**	**Overweight**	**Mild obesity**	**Moderate obesity**	**Extreme obesity**
	≤18.5	**18.5~25**	**25~30**	**30~35**	**35~40**	**≥40**
PA for entire projection area(mm^2)	**3168**	**3184**	**3235**	**3302**	**3369**	**3706**
V for proximal femur volume(mm^3)	**95586**	**96411**	**98774**	**102341**	**105538**	**117569**
$vBMD_{trab}$(g/cm^3)	**0.203 ±0.038**	**0.219 ±0.028**	**0.233 ±0.026**	**0.241 ±0.034**	**0.253 ±0.040**	**0.260 ±0.040**

The first two rows of data are measured from the model so there is no standard deviation value.

The cortical bone of the proximal femur takes most of the load in a sideways fall since it has a much larger stiffness comparing to that of trabecular bone. Thus, only the cortical bone's strength is compared with maximum von Mises stress in the simulation as stress oriented failure criterion.

CHAPTER 5

PROBABILITY APPROACH

5.1 Margin of Safety Method

The margin of safety method which is commonly used in engineering field as reliability assessment is recently introduced in the biomechanics field (Easley et al., 2007) to quantify the probability of failure and sensitivity analysis. In this study we assume that natural, un-interfered events obey Gaussian distribution, which provides a solid approach to probability density functions of the maximum von Mises stress and femoral strength. If we denote x as a random variable with mean value μ and standard deviation σ, its probability density function (pdf) is

$$pdf(x) = \frac{1}{\sqrt{2\pi\sigma^2}} e^{-\frac{1}{2}\left(\frac{x-\mu}{\sigma}\right)^2} \tag{18}$$

Let S be a random variable representing ultimate bone strength and $(\sigma_{vm})_{\max}$ be a random variable representing maximum von Mises stress in the bone as illustrated in Figure 0.1.

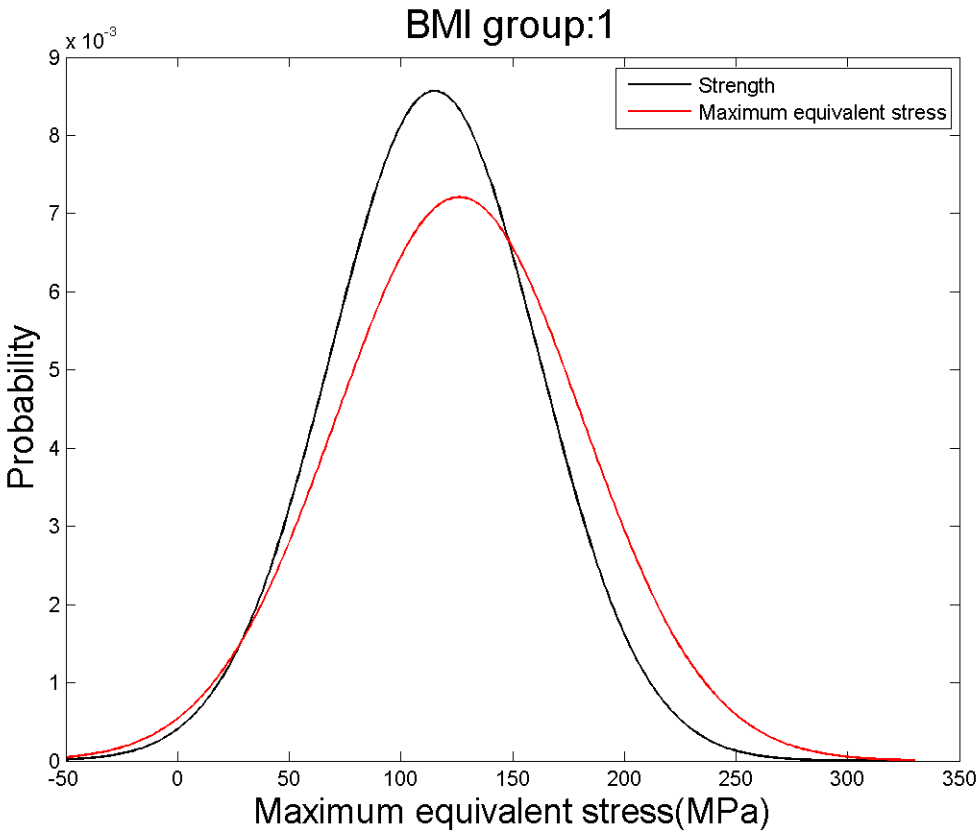

Figure 0.1 Illustration of strength and maximum von Mises stress in bone of Cohort 1.

Although the bone is heterogeneous with strength varying somewhat spatially, we will assume bone strength is homogeneous here because such variation within an individual's bone is ignored. Z is introduced as a dependent random variable as the margin of safety by

$$Z = S - (\sigma_{vm})_{\max} \tag{19}$$

When Z is less than zero, stress exceeds strength at the location of maximum von Mises stress and bone failure will occur. Since Z is stochastic with a given pdf, the probability of bone failure is given by integrating the pdf of Z (i.e. summing up) for all possible values of Z<0:

$$probability\ of\ failure = \int_{-\infty}^{0} pdf(Z)dZ \tag{20}$$

The transition functions are used to calculate the variation of each variable in this research either through direct observation or transition function from existing variables.

5.2 Transition functions for random variables

The mathematical relationships between the body conditions from direct observations of the cohort and intermediate variables for the sideways fall are conducted above, all of which are in form of random variables. The distributions of dependent random variables require transition functions to convert from independent random variables.

If we denote the mean value of a random variable x as μ_x (i.e. $\mu_x \equiv E[x]$), its standard deviation as σ_x, and pdf(x) is the probability density function of x, then the variation of x is

$$Var(x) = \sigma_x^2 = \int_{\infty}^{\infty} (x-\mu)^2 pdf(x) dx \tag{21}$$

If another random variable y is a function of x, say $y = f(x)$. The mean value and variation of y would be:

$$\mu_y = f(\mu_x) + \frac{1}{2}\frac{d^2 f}{dx^2}\Big|_{\mu_x} \sigma_x^2 \tag{22}$$

$$Var(y) \equiv \sigma_y^2 \approx \left\{ \left(\frac{df}{dx}\Big|_{\mu_x} \right)^2 - f(\mu_x)\frac{d^2 f}{dx^2}\Big|_{\mu_x} \right\} \sigma_x^2 \tag{23}$$

Usually the second derivative terms of the Eqn.(22) and (23) are negligible therefore a simplified form follows:

$$\mu_y = f(\mu_x) \tag{24}$$

$$Var(y) = \sigma_y^2 \approx \left(\frac{df}{dx}\Big|_{\mu_x} \cdot \sigma_x\right)^2 \tag{25}$$

There is a natural extension of this formula for multi-variable functions. Let y be a function of n independent random variables xi: $y = f(x_1, x_2, \ldots, x_n)$ by G.E. Dieter and L.C. Schmidt et al. (Dieter & Schmidt, 2013).

$$\mu_y = f(\mu_{x_1}, \mu_{x_2}, \cdots, \mu_{x_n}) \tag{26}$$

$$Var(y) = \sigma_y^2 \approx \sum_{i=1}^{n} \left(\frac{\partial f}{\partial x_i}\Big|_{\underset{\sim}{\mu}_x} \cdot \sigma_{x_i}\right)^2 \tag{27}$$

where the $\Big|_{\underset{\sim}{\mu}_x}$ notation in the Eqn.(27) indicates that the partial derivative of the function with respect to each independent random variable x_i is evaluated at the mean values of all the independent random variables.

5.3 Six Sigma Analysis

In ANSYS®, the probabilistic function is achieved through the six sigma component which samples the specified data domain to generate a response surface and evaluate the contributions from each of them. CCD(central composite design) method is adopted to sample the data domains which are peak fall force, Young's modulus of cortical bone and trabecular bone in this study.

If we take the 3 variables as axes to form a Cartesian coordinate space, the mean values of each variable would coincide with each other to mark the origin. The positive and negative alpha values of all 3 axes form a cube in the coordinate space. The face centered CCD method will sample the corresponding value of the coordinate from 8 vertices of the cube, 6 center point of each face and the origin point. Considering the data domain of Gaussian distributed random variables, the alpha value is taken as 3.09 times of the standard deviation as the upper and lower boundaries by the system.

CHAPTER 6

BMI DOMINATED RESULTS FOR HEALTHY FEMUR

6.1 Mesh and Convergence

Finite element analysis yields an approximate solution to the governing problem, the accuracy of which is improved with mesh refinement by a series of analysis with different level of meshing. The simulation of Cohort 1 was performed with 3mm averaged mesh size and 15945 elements as an initial mesh in Figure 0.1.

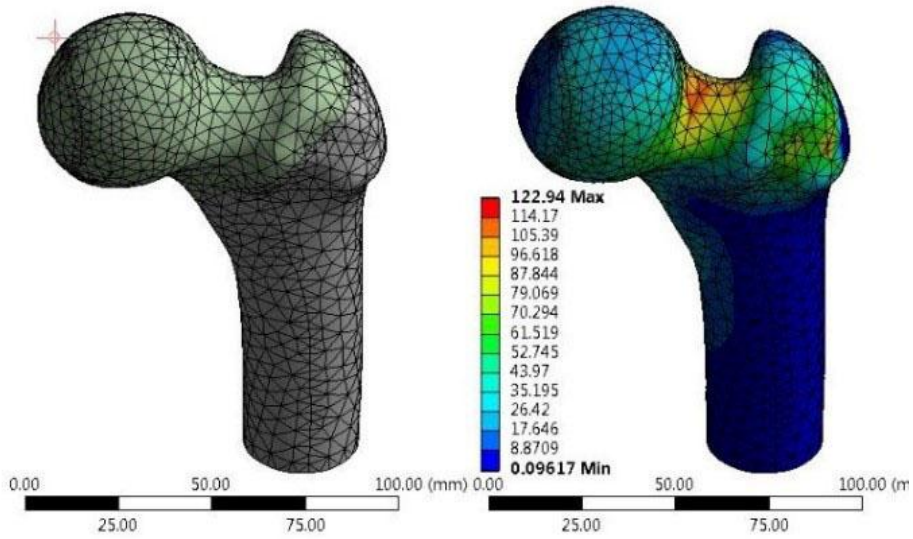

Figure 0.1 Initial mesh for the femur bone from Cohort 1.

The preliminary result helps geometry sectioning to focus on the region of interest and the convergence study. As illustrated the von Mises stress in the femoral neck region is much higher than elsewhere in the proximal femur. Thus, the model is sectioned at the intertrochanter region for the efficiency of local mesh refinement to the femoral head and neck region.

As seen in Figure 0.2 the mesh refinement is performed in the femoral neck region to approach the convergence limit. After the second local mesh refinement, the total element number rise from 24313 to 47425 and the maximum von Mises stress goes from 125.61MPa to 126.20MPa, which has a final change of 0.4743%.

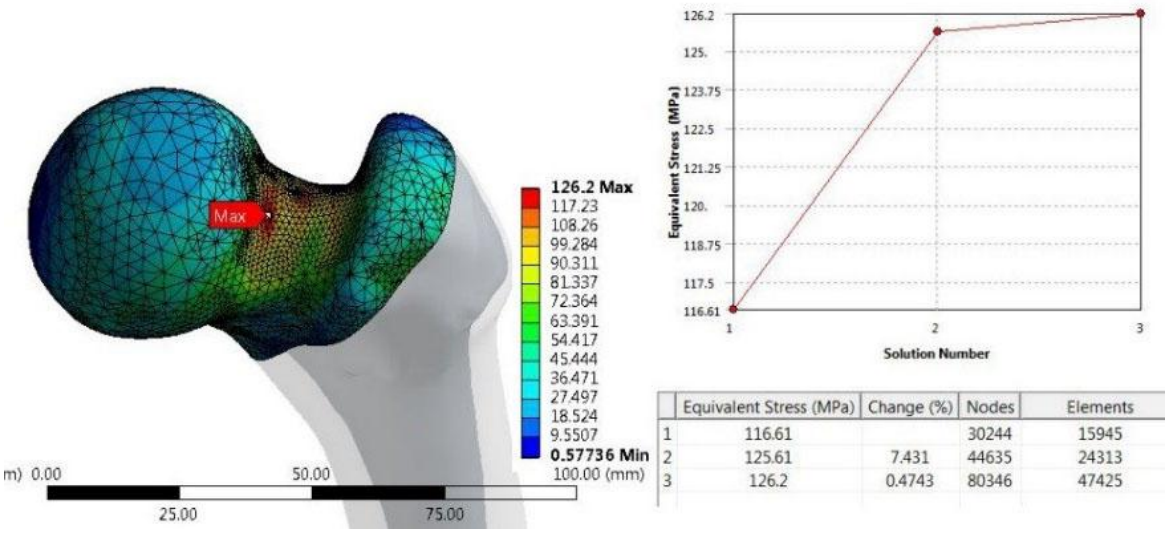

	Equivalent Stress (MPa)	Change (%)	Nodes	Elements
1	116.61		30244	15945
2	125.61	7.431	44635	24313
3	126.2	0.4743	80346	47425

Figure 0.2 Mesh convergence result of Cohort 1.

In the same manner, each cohort is performed with a convergence study and the result of mesh refinement and von Mises stress is shown in Figure 0.3 with the converged result of maximum von Mises stress. The differences among cohorts are primarily reflected on the maximum values of von Mises stress instead of stress distributions among the anatomical sites. Under the padding effect of the soft tissue, the maximum von Mises stress is found to decrease with increasing BMI, though the rate of which becomes smaller.

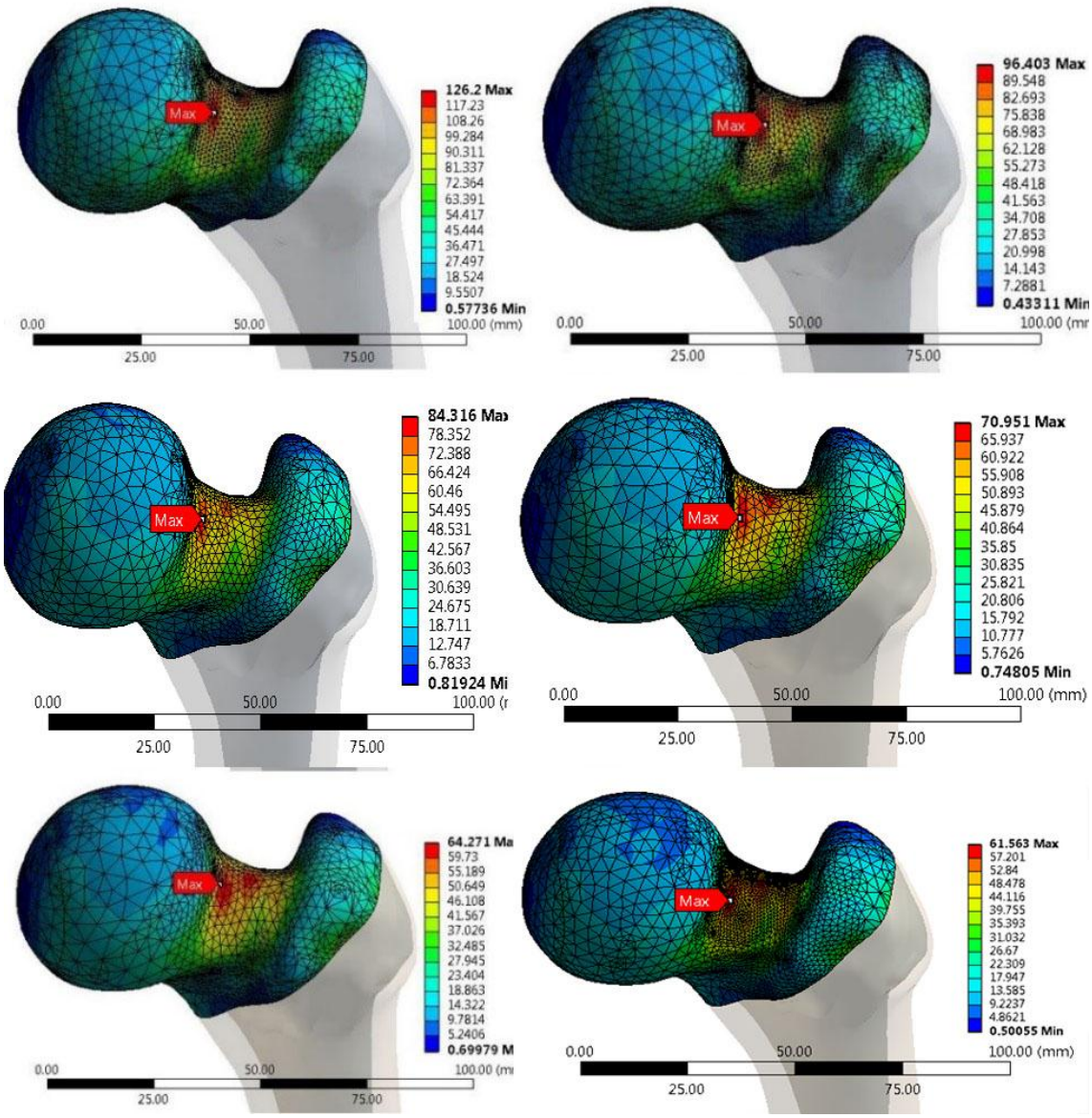

Figure 0.3 Deterministic results of the 6 cohorts with mean values of input parameters. The final changes of maximum von Mises stress of convergence study for Cohort 2-6 are: 0.5968%, 1.8773%, 1.0661%, -0.1244%, 0.9208% respectively.

6.2 Probability density functions of stress and strength

In the ANSYS® Six Sigma Analysis, Release 17.2, the three input parameters which are peak fall force, cortical bone and trabecular bone elastic modulus are treated as continuous random variables with normal distributions. Experiments are designed by

sampling these variables under CCD(central composite design) method. The scheme of Six sigma component with Parameter Set is shown in Figure 0.4.

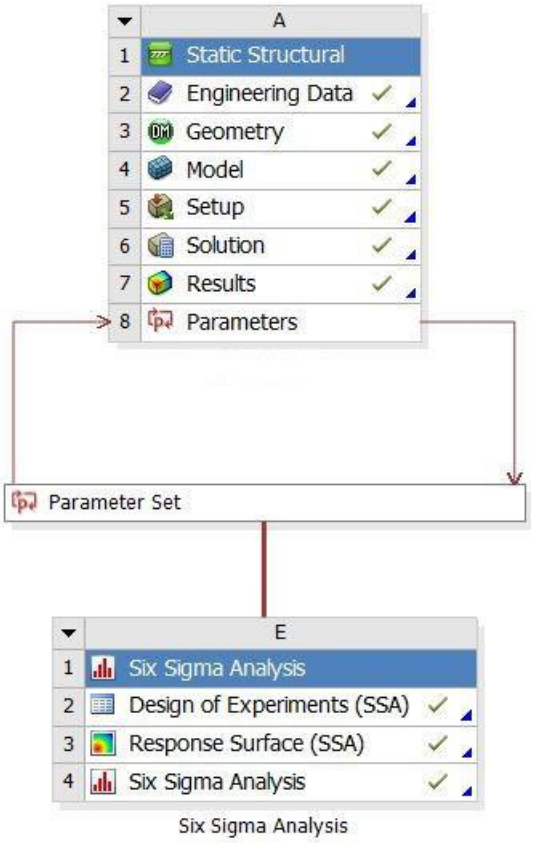

Figure 0.4 The Six sigma analysis scheme.

The sampling points of Cohort 1 is shown in Figure 0.5 where the input parameters are from Table 0.2, Table 0.4 and Table 0.6 for further calculation.

Table 0.6 respectively.

Table of Schematic C2: Design of Experiments (SSA) (Central Composite Design : Face-Centered : Standard)

	A	B	C	D	E
1	Name	P17 - cortical (Pa)	P18 - trabecular (Pa)	P19 - Force X Component (N)	P16 - Equivalent Stress Maximum Maximum Value Over Time (MPa)
2	1	7.9722E+09	6.34E+08	5207	127.89
3	2	1.7621E+08	6.34E+08	5207	15.544
4	3	1.5768E+10	6.34E+08	5207	153.61
5	4	7.9722E+09	8.7029E+07	5207	268.61
6	5	7.9722E+09	1.181E+09	5207	105.85
7	6	7.9722E+09	6.34E+08	4264.5	104.74
8	7	7.9722E+09	6.34E+08	6149.5	151.04
9	8	1.7621E+08	8.7029E+07	4264.5	50.975
10	9	1.5768E+10	8.7029E+07	4264.5	305.55
11	10	1.7621E+08	1.181E+09	4264.5	7.693
12	11	1.5768E+10	1.181E+09	4264.5	106.44
13	12	1.7621E+08	8.7029E+07	6149.5	73.507
14	13	1.5768E+10	8.7029E+07	6149.5	440.62
15	14	1.7621E+08	1.181E+09	6149.5	11.094
16	15	1.5768E+10	1.181E+09	6149.5	153.48

Figure 0.5 Sample points of Cohort 1 in six sigma analysis.

The respond surface with respect to the maximum von Mises stress result is shown in Figure 0.6. The three input variables are plotted in pairs in 3D diagrams.

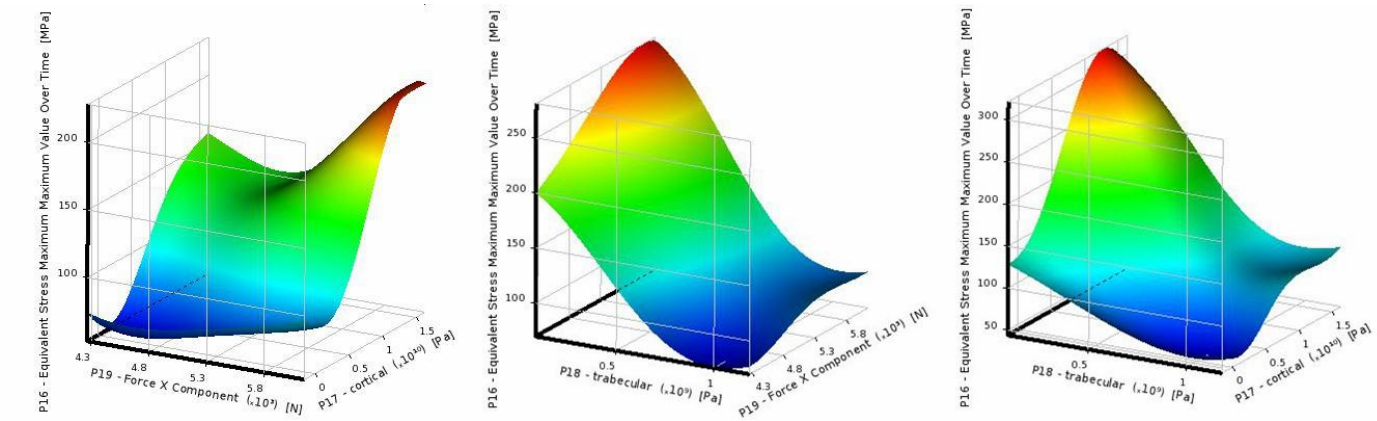

Figure 0.6 Response surface with respect to maximum von Mises stress.

The mean value and standard deviation of the maximum von Mises stress and cortical bone strength for each cohort is presented in Table 0.1.

Table 0.1 Maximum von Mises stress and the cortical bone strength.

	BMI categories					
	Underweight	Healthy weight	Overweight	Mild Obesity	Moderate Obesity	Extreme Obesity
Stress	126.1±47.45	92.07±16.60	82.96±11.99	71.32±13.94	61.53±15.58	59.03±13.69
Strength	115.0±46.56	115.0±36.25	115.0±33.20	114.9±37.82	115.0±39.83	115.0±39.27

To illustrate the comparison between them, the probability density functions of bone strength and maximum von Mises stress are plotted with MATLAB® (The MathWorks, Inc. Natick, MA) in Figure 0.7.

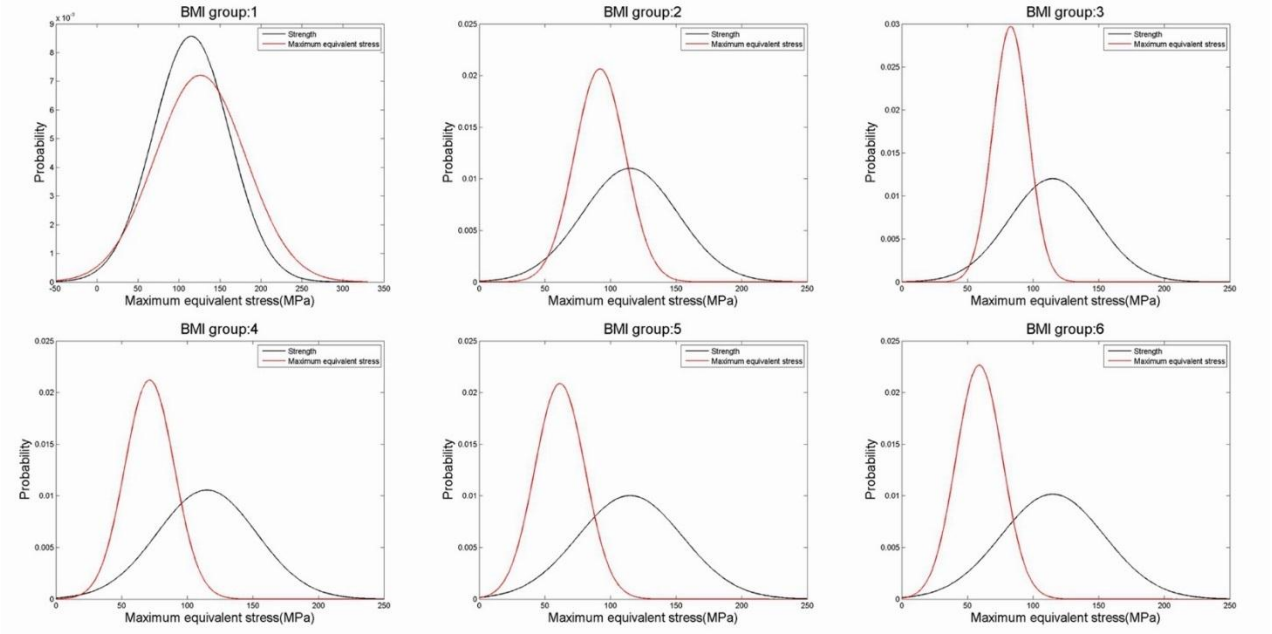

Figure 0.7 the probability density function curves of the 6 BMI cohorts.

The distributions of first two cohorts are relative scattered because of the wide range of BMI for Cohort 1(BMI:0~18.5) and the vast number of subjects for Cohort 2(normal weight cohort). For each cohort the margin of safety probability Z is obtained through

Eqn. (19) and the probability of failure was calculated according to Eqn. (20). Table 0.2 shows the probability result of different BMI cohorts.

Table 0.2. Results from different methods in predicting the likelihood of hip fracture in a sideways fall.

	BMI categories					
	Underweight	Healthy weight	Overweight	Mild Obesity	Moderate Obesity	Extreme Obesity
	≤18.5	18.5~25	25~30	30~35	35~40	≥40
Predicted probability of failure	56.89%	28.67%	18.56%	14.21%	10.77%	9.10%

For the underweight cohort, the probability of failure is 56.89% while the probability for normal weight cohort is 28.67% where a huge drop is observed here considering the average BMI for the 2 cohorts are 17.51 and 22.56. The probabilities of failure for Cohort 3, 4, 5 and 6 are 18.56%, 14.21%, 10.77% and 9.10% respectively with relatively small changes between adjacent cohorts. Throughout the entire BMI category, there is a large difference of the probability of failure that the Cohort 1 has a roughly 6 times of Cohort 6's chance to get a hip fracture in such a sideways fall. Several variables such as peak fall force and maximum von Mises stress were used as indicators predicting the likelihood for a hip fracture in sideways fall by previous researches(Bouxsein et al., 2007)(Mayhew et al., 2005) and they are reinvestigated here to address the role of BMI in affecting the sideways fall.

6.3 Comparison between force and stress dominated prediction

Several variables such as peak fall force and maximum von Mises stress were used as indicators in predicting the likelihood for a hip fracture in sideways fall by previous researchers(Bouxsein et al., 2007)(Mayhew et al., 2005). Since BMI is the dominating

factor of interest, the results of force and stress of all cohorts are normalized by dividing the peak force and maximum equivalent stress for each cohort by the value of Cohort 1 (BMI < 18.5) and plotted in Figure 0.8 for comparison.

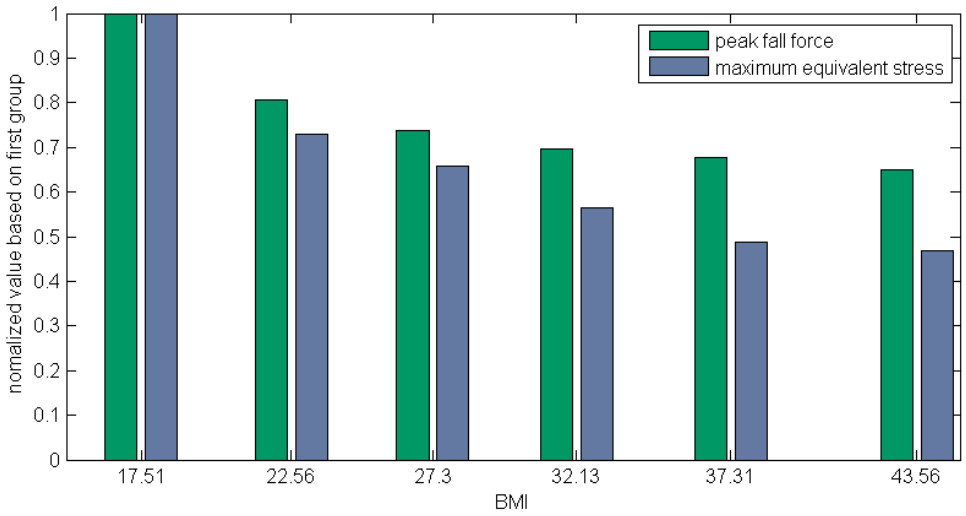

Figure 0.8 Normalized peak fall force and maximum von Mises stress predicted.

Both variables have negative correlation with BMI, while the maximum von Mises stress is decreasing faster than peak fall force as for higher BMI cohorts. The peak fall force of Cohort 6(extreme obesity) is around 65% the value of Cohort 1 but the maximum von Mises stress result of Cohort 6 is only about 47% of that from Cohort 1. Such divergence of the two curves especially for high BMI cohorts illustrate the effect of the geometry expansion and elastic modulus difference for bone material which were not included in the stage of peak fall force calculation.

6.4 Margin of Safety predicted probability, Factor of risk and relative incident rate

The relative fracture incidents per 1000 person-year (hip region only) adjusted for age, hormone use and diabetes is reported by BMI category from the identical literature(Beck et al., 2009). Each cohort of NHW women in WHI-OS is recorded in Table 0.3.

Table 0.3. Relative incidents and the predicted probability of failure.

	BMI categories					
	Underweight	**Healthy weight**	**Overweight**	**Mild Obesity**	**Moderate Obesity**	**Extreme Obesity**
	≤18.5	**18.5~25**	**25~30**	**30~35**	**35~40**	**≥40**
Probability of failure	61.87%	36.60%	24.11%	18.50%	16.11%	12.70%
Incidents/thousand-person year	4.743	2.168	1.503	1.221	1.212	0.930
Factor of risk based on stress	1.096	0.8004	0.7213	0.6202	0.5349	0.5131

The Factor of risk is the ratio between maximum von Mises stress and the bone strength of each cohort which is presented here as the comparison between deterministic approach and probability based approach.

The variables in Table 0.3 are normalized based on the value of the Cohort 1 and plotted in Figure 0.9 for comparison.

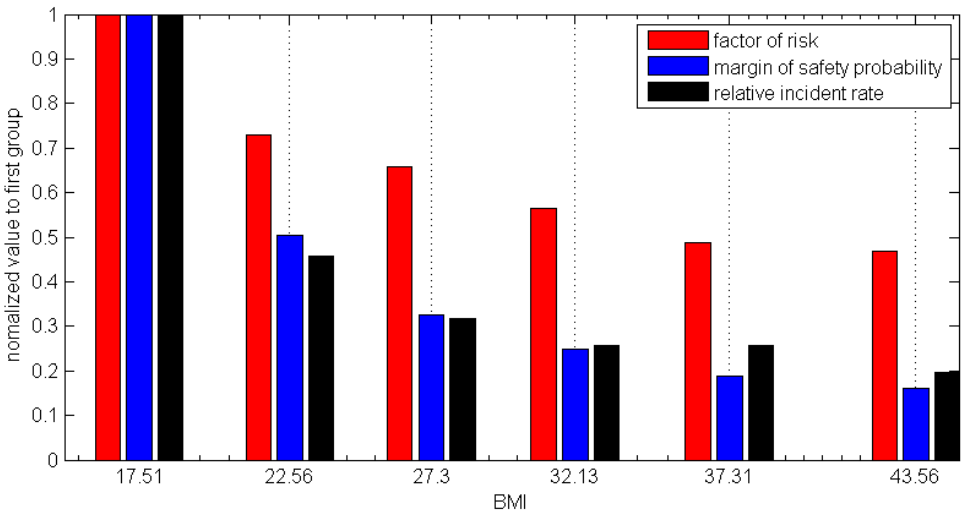

Figure 0.9 Normalized margin of safety probability, factor of risk and relative incident rate.

The red bars representing the factor of risk based on maximum von Mises stress and bone strength are significantly overestimating the likelihood of hip fracture for higher BMI cohorts comparing with the reported incident rate.

However, the margin of safety predicted probability of failure shows very similar value in describing such relative changes among cohorts due to BMI, both of which have a huge drop as for higher BMI cohorts comparing to normalized force and stress curves. The values for the first four cohorts are considered well fitted while a small divergence was observed for the last two cohorts. We speculate there are two major reasons behind such divergence between statistics and the model. First, other factor such as daily activity patterns of the subjects are changing greatly for such high BMI cohorts. Second, the lack of enough samples for a good conclusion could be the reason where there are only a few subjects in the two cohorts and fewer experienced a hip fracture.

In summary, the margin of safety method explains the role of BMI from the probability approach coupled with finite-element method which is well fitted with the reported record comparing to the deterministic approach. After the probabilistic approach application on the BMI influence being confirmed, it is ready to introduce another factor into the sideways fall: the tumor lesion.

CHAPTER 7

TUMOR AFFECTED RESULTS

7.1 Parameterization of Tumor Lesions

Certain parameterizations are made with simplifications in describing tumor lesions of this study. The parameterization of tumor lesions only considers the size and location information while the variety of tumor lesion shape is ignored because of the difficulty in describing the tumor morphology with one or two simple parameters. Thus, all the tumor lesions are idealized as spherical holes with center point through the cortical bone shell as the shown in Figure 0.1.

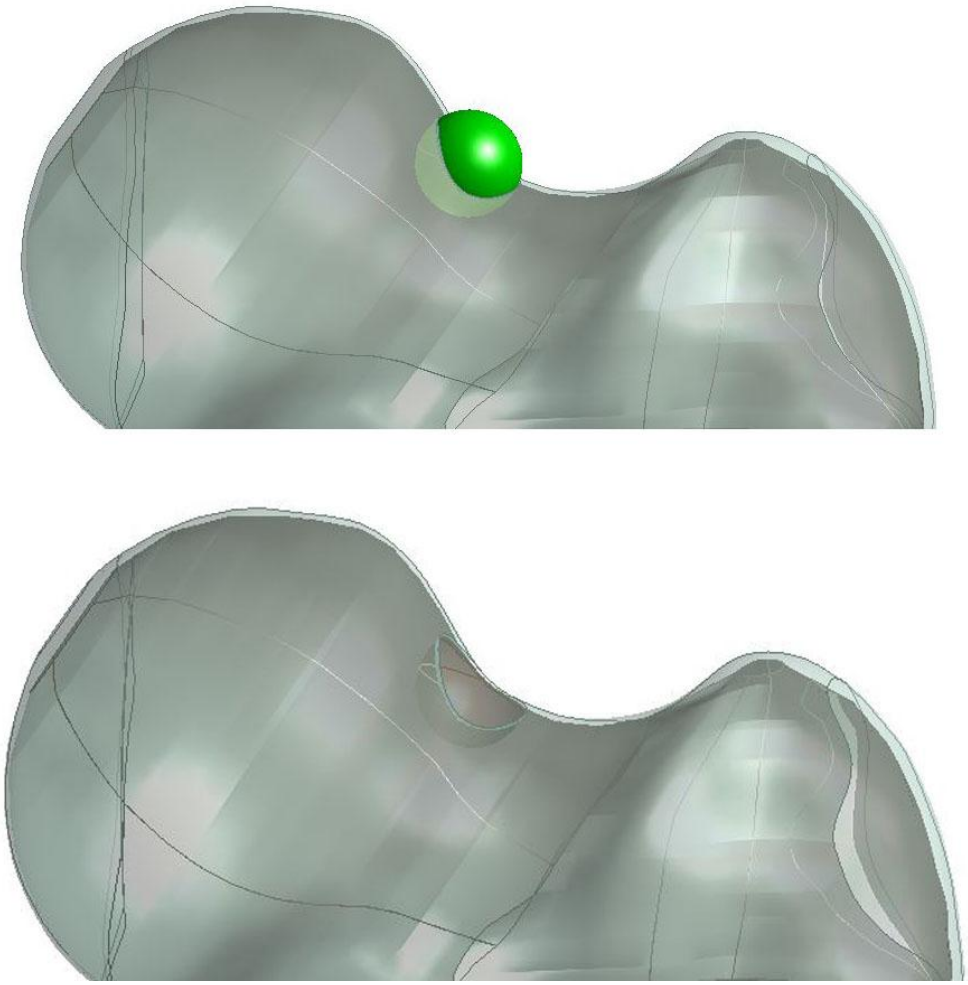

Figure 0.1 Illustration of tumor lesion's creation and effect in proximal femur bone.

It is hypothesized that the influence of tumor lesion in terms of probability failure is location sensitive due to the complexity and irregularity of proximal femur bone. Five typical anatomical locations are selected to place tumor lesions in Figure 0.2 which are superior side of femoral head, superior/anterior(because it is a left femur)/inferior side of femoral neck and superior side of intertrochanter region.

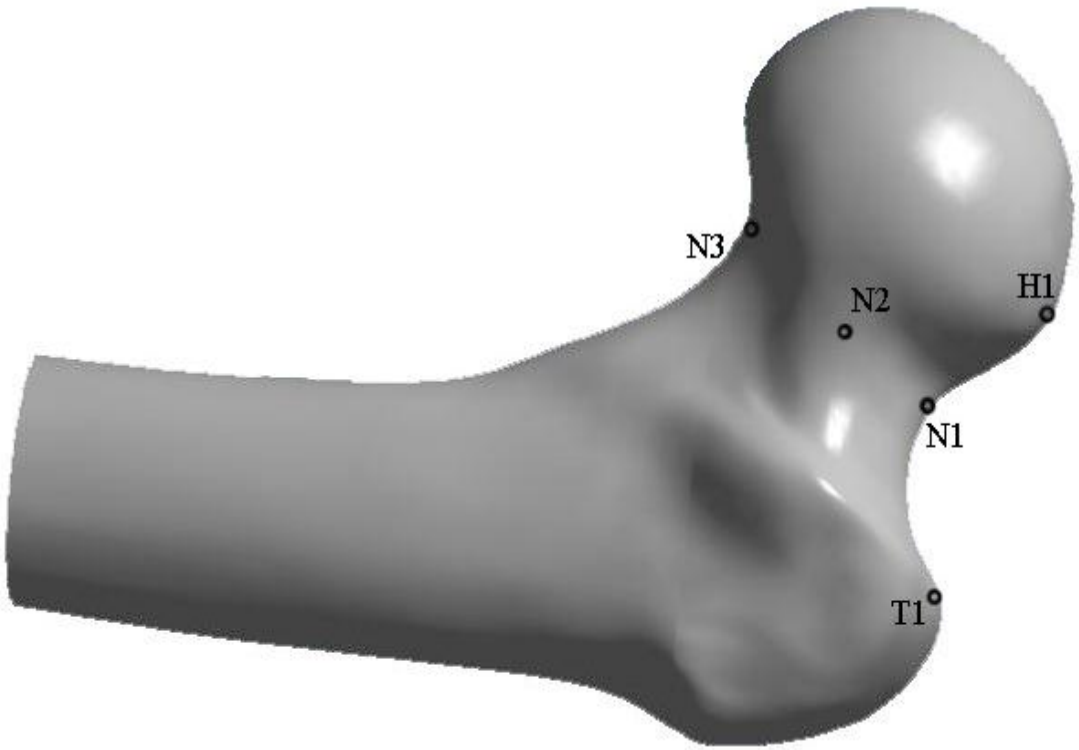

Figure 0.2 Illustration of tumor lesion locations.

For each lesion site in this study, the lesion diameter varies from 0 mm (healthy) to 20mm with an increment of 4mm, representing the severity of lesion damage. There are six sizes of tumor lesions for each tumor location and five anatomical locations for each BMI cohort, resulting in 180 unique situations to be simulated and recorded.

7.2 Stress Concentration Effect and factors

Due to the irregularity of an object like holes and notches that the stress could be increased locally under certain load condition and the ratio of concentrated stress and nominal stress is called stress concentration factor(Young & Budynas, 2002). However, a stress concentration factor is usually discussed in simple 1-D type mechanics problems to estimate the maximum value of normal or shear stress for simple shapes and loading conditions. Here, we extend this concept to the 3D stress tensor field by developing FEA-determined stress concentration factors as a function of lesion size and location which is

applied to the stress metric best correlated to bone failure von Mises stress. function K_t is then defined as:

$$K_t = \frac{\max \sigma_{vm}(D, \vec{x_i})}{\max \sigma_{vm}(0, \vec{x_0})} \tag{28}$$

where D is the diameter of a lesion hole and $\vec{x_i}$ indicates the location of maximum von Mises stress in a lesion affected bone. $\sigma_{vm}(0, \vec{x_0})$ is the value of maximum von Mises stress in healthy bone (i.e. D = 0) and x_0 indicates the location of the maximum von Mises stress.

The material property of cortical and trabecular bone is linear for the study that the analysis is also linear with the input parameters in such a static type of simulation. In order to simplify all the 180 simulations from six BMI cohorts, stress concentration factors are made to describe the influence of tumor lesion comparing to the healthy ones. The maximum von Mises stress of tumor damaged situations are divided by those from corresponding healthy ones to yield the stress concentration factors that each of them is able to represent a unique tumor damaged situation in the simulation.

That is, for a given tumor lesion location and size, the maximum von Mises stress can be determined by the factor with respect to healthy bone's result from the corresponding BMI cohort. Figure 0.3 shows the stress concentration factors for the 5 selected sites with different lesion sizes.

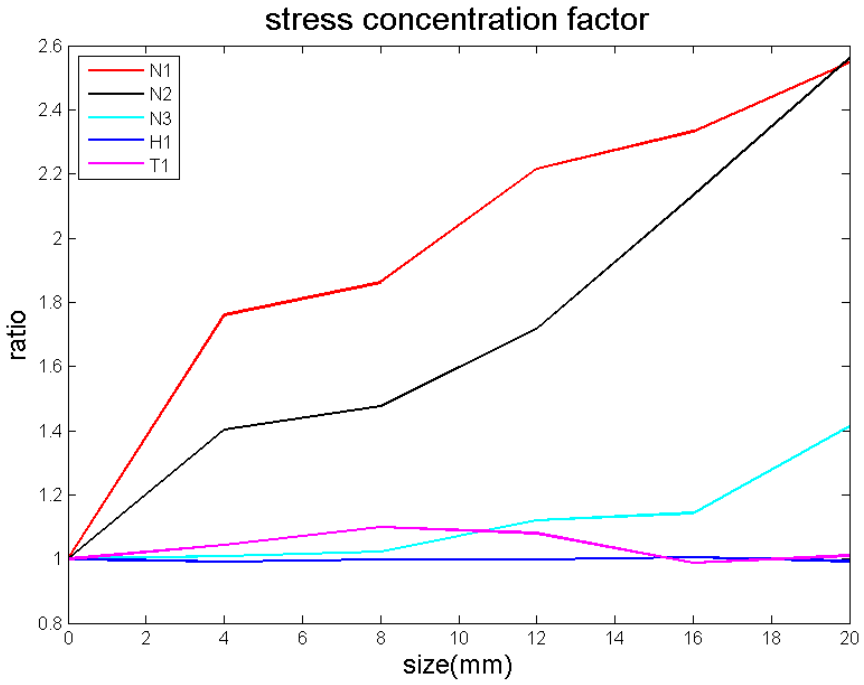

Figure 0.3 stress concentration factor curves of tumor lesions.

As seen above, the existence of tumor lesion in N1 and N2 has a significant influence to the maximum von Mises stress result. The 4mm's tumor lesion causes a 1.8 times rise of maximum von Mises stress to location N1 and 1.4 times to N2. Eventually the stress rise reaches roughly 2.6 times for both of them. The inferior side of the femoral neck is less sensitive to the tumor lesion that the factor is below 1.2 when it is smaller than 16mm. When the lesion diameter reaches a critical point of 20mm, the maximum von Mises stress then rises to 1.4 times to that of healthy one. In the femoral head region, tumor lesion has negligible influence of the maximum von Mises stress in such a sideways fall. The tumor lesion at superior side of intertrochanter region has slight influence on the maximum von Mises stress and a negative correlation with maximum von Mises stress when the diameter is larger than 8mm.

7.3 Probability density function(pdf) curves

The probability density functions(pdf) for different tumor lesion conditions are referred to corresponding healthy subjects' (pdf) in Figure 0.7 and stress concentration factors in Figure 0.3. The two results are incorporated through the transition functions to yield the mean value and standard deviation of maximum von Mises stress.

In Figure 0.4, Figure 0.5, Figure 0.6, Figure 0.7 and Figure 0.8, the probability density function curves of maximum von Mises stress with different lesion diameters are plotted with different colors. Because the stress concentration factors are usually greater than one that tumor damaged probability density function curves are usually wider than normal (i.e. greater standard deviation) which means the distribution of possible maximum von Mises stress are more scattered.

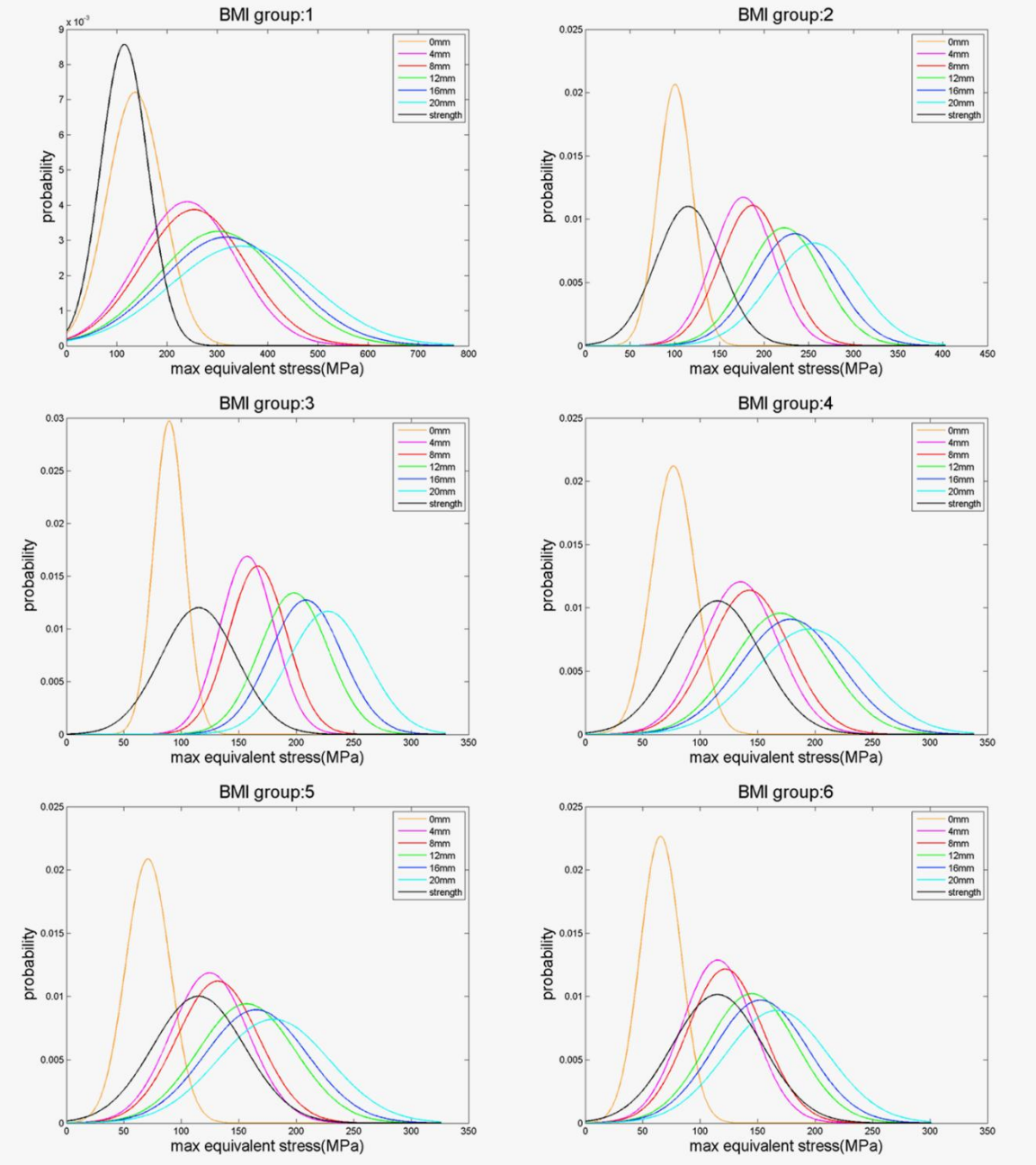

Figure 0.4 maximum von Mises stress probability density function curves for tumors on superior region femoral neck.

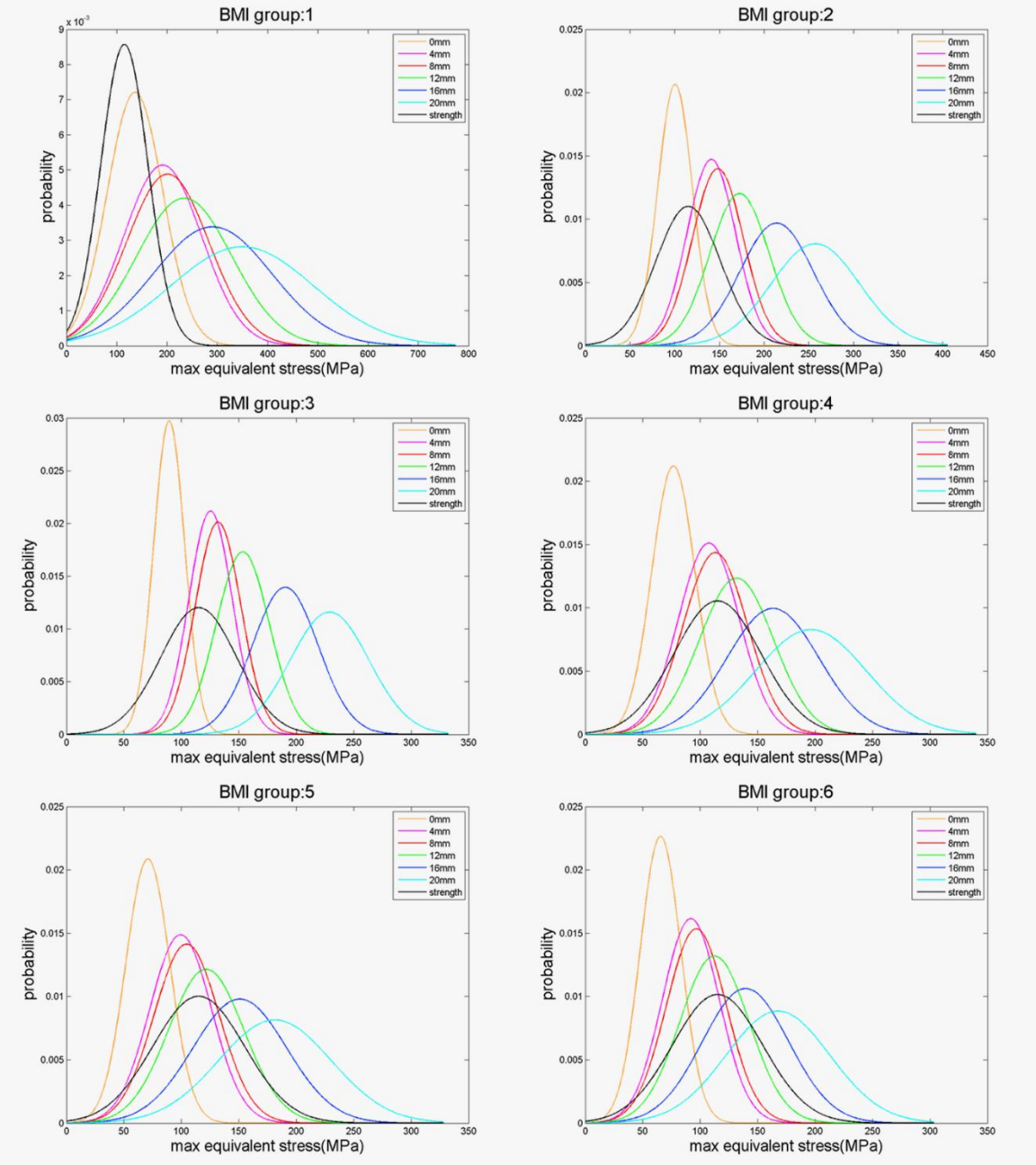

Figure 0.5 maximum von Mises stress probability density function curves for tumors on the side region of femoral neck.

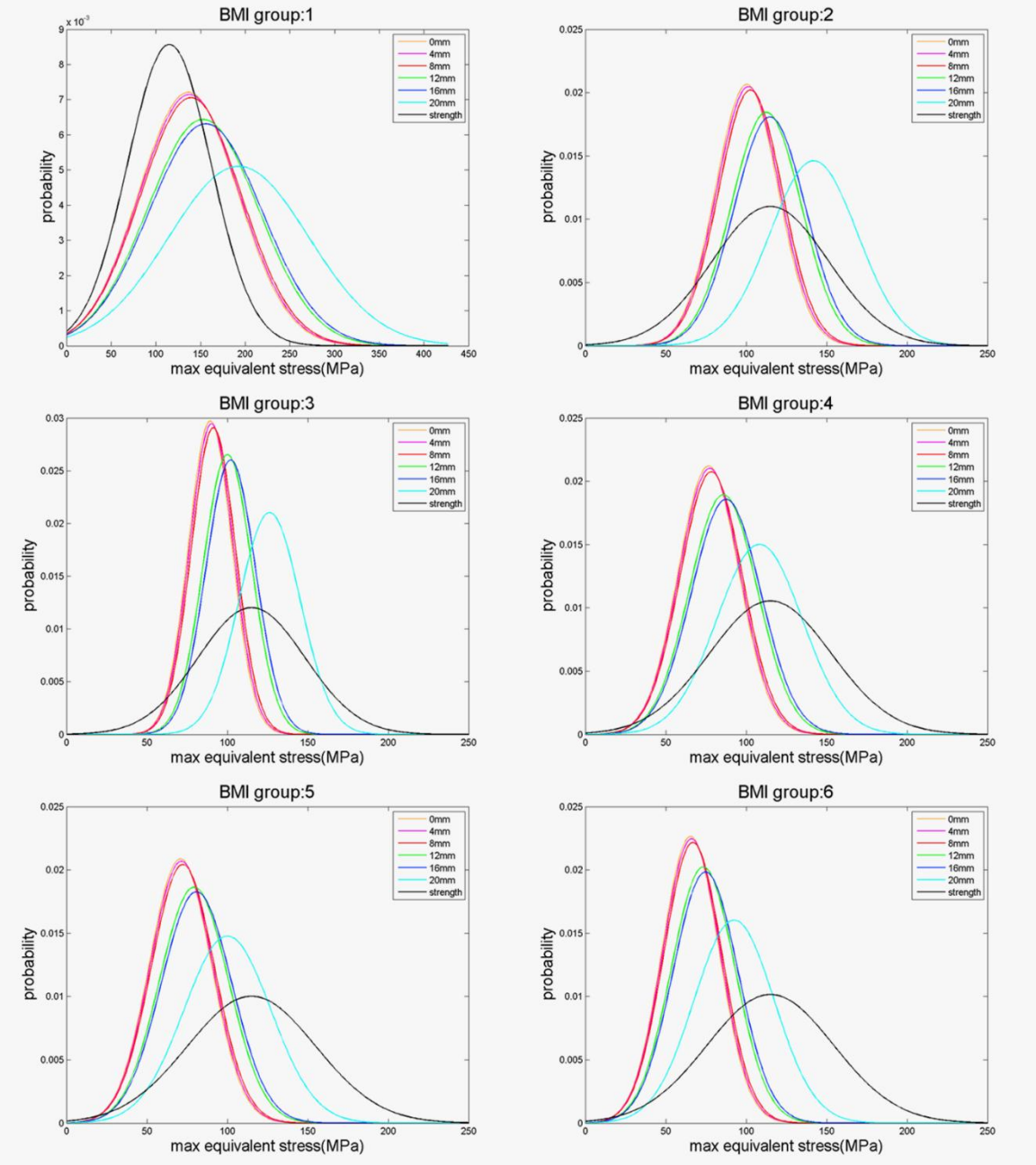

Figure 0.6 maximum von Mises stress probability density function curves for tumors on inferior region femoral neck.

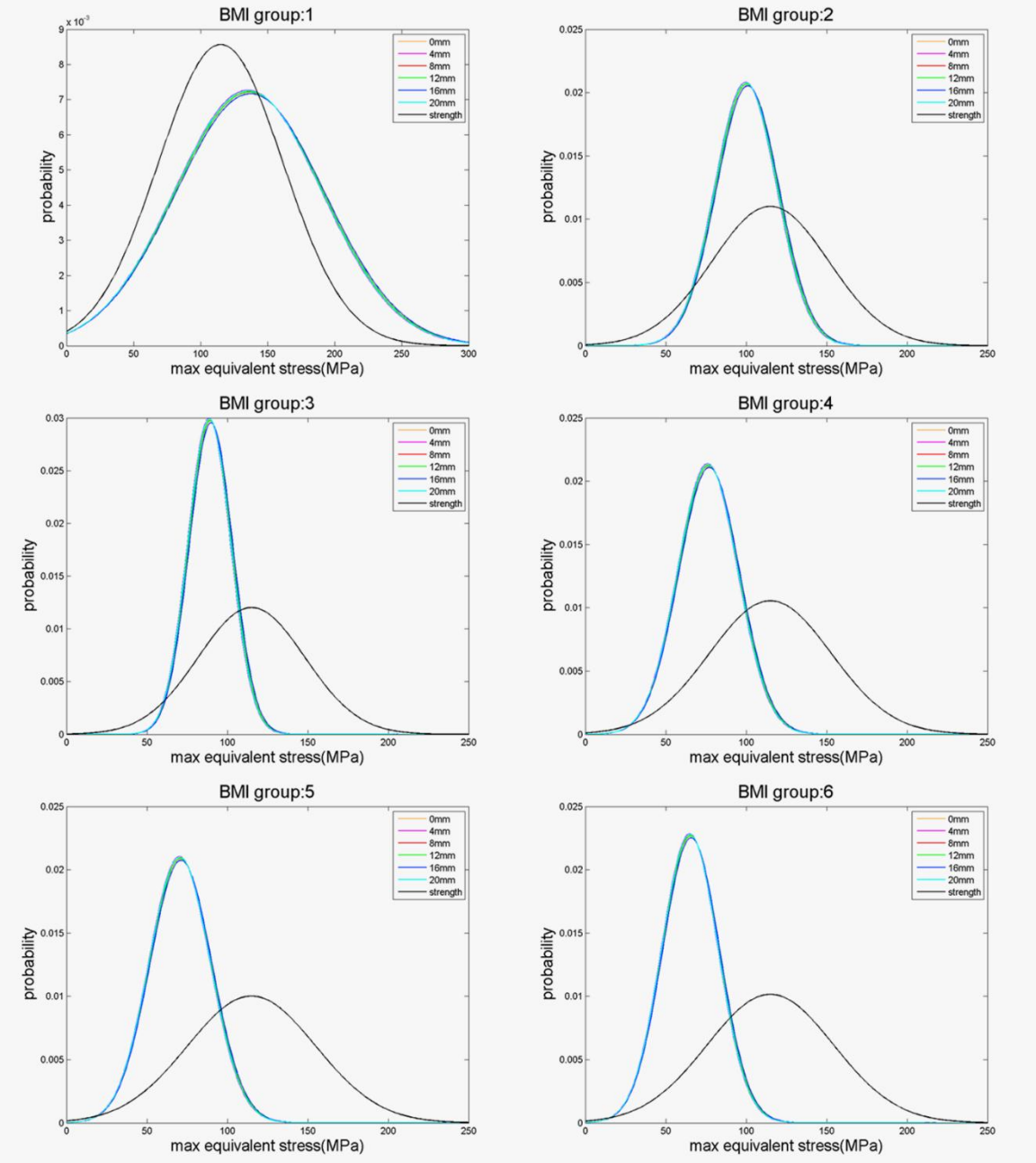

Figure 0.7 maximum von Mises stress probability density function curves for tumors on superior region of femoral head.

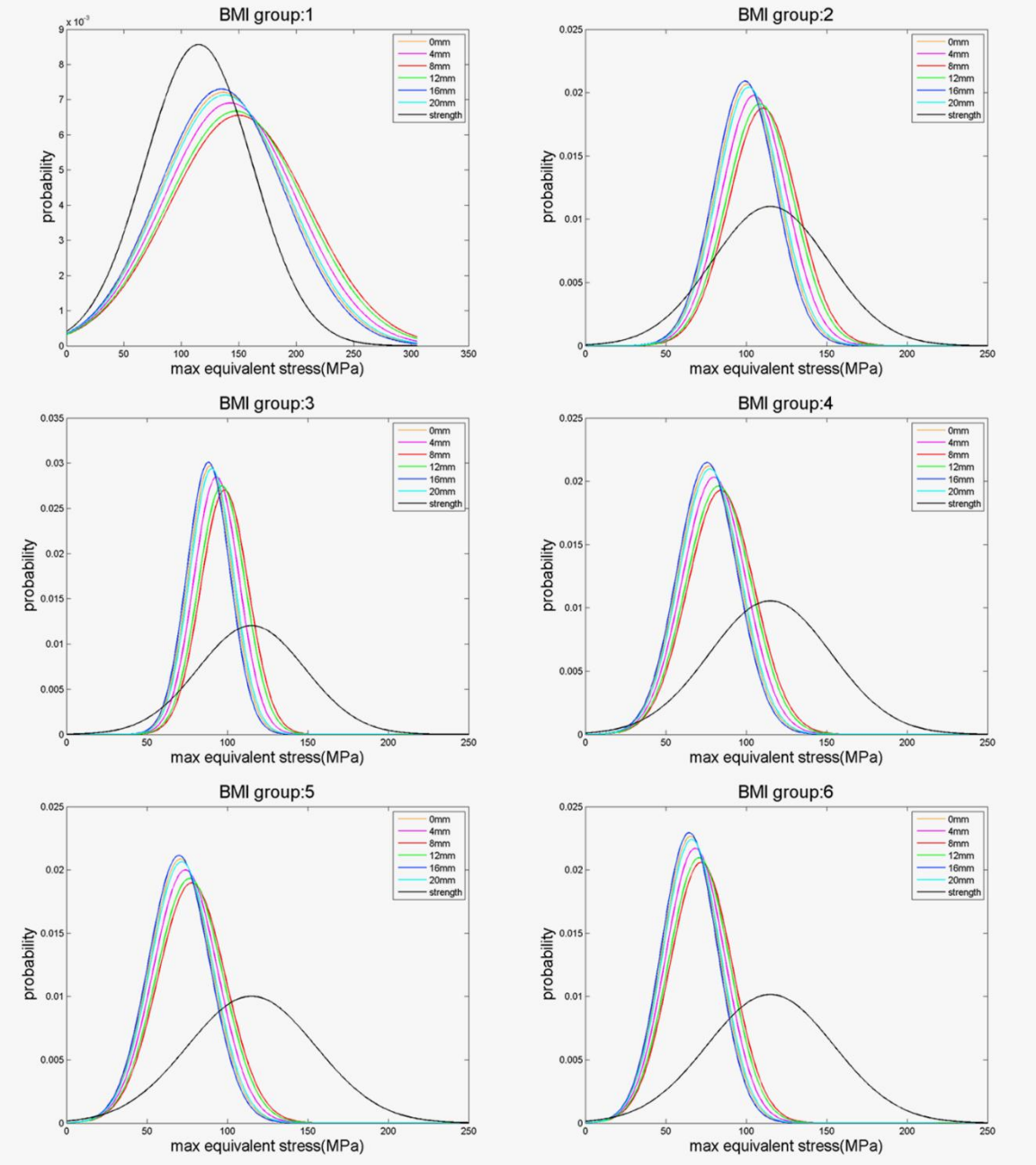

Figure 0.8 maximum von Mises stress probability density function curves for tumors on trochanteric region of femur.

7.4 Failure probabilities for tumor damaged femurs

Through the integral function from Eqn.(20), all the possibilities with a negative value (bone strength is smaller than the stress load at the given possibility) for each situation are summed up to yield a probability of failure.

For the convenience of comparison and analysis, the probabilities of failure for each situation is summarized in Table 0.1.

Table 0.1 Probability of failures based on BMI categories, lesion locations and lesion sizes.

		BMI categories(kg/m2)					
	Lesion size(mm)	Underweight ≤18.5	Healthy weight 18.5~25	Overweight 25~30	Mild Obesity 30~35	Moderate Obesity 35~40	Extreme Obesity ≥40
N1	0	56.89%	28.67%	18.56%	14.21%	10.77%	9.10%
	4	86.92%	84.62%	78.81%	59.64%	44.86%	40.85%
	8	88.56%	88.39%	84.10%	65.50%	50.04%	46.06%
	12	92.41%	95.84%	94.84%	81.36%	66.04%	62.83%
	16	93.25%	97.06%	96.55%	85.06%	70.44%	67.60%
	20	94.46%	98.44%	98.40%	90.22%	77.34%	75.21%
N2	0	56.89%	28.67%	18.56%	14.21%	10.77%	9.10%
	4	77.86%	63.31%	52.00%	36.73%	26.74%	23.41%
	8	80.27%	68.78%	58.38%	41.54%	30.34%	26.76%
	12	86.14%	82.77%	76.28%	57.08%	42.68%	38.68%
	16	91.69%	94.66%	93.13%	78.20%	62.54%	59.08%
	20	94.54%	98.51%	98.49%	90.52%	77.78%	75.71%
N3	0	56.89%	28.67%	18.56%	14.21%	10.77%	9.10%
	4	57.52%	29.41%	19.15%	14.59%	11.03%	9.33%
	8	58.41%	30.47%	20.02%	15.15%	11.43%	9.67%
	12	64.71%	38.98%	27.31%	19.88%	14.71%	12.54%
	16	65.99%	40.95%	29.10%	21.04%	15.52%	13.25%
	20	78.22%	64.11%	52.91%	37.40%	27.24%	23.86%
H1	0	56.89%	28.67%	18.56%	14.21%	10.77%	9.10%
	4	56.31%	28.00%	18.03%	13.86%	10.53%	8.89%
	8	56.76%	28.52%	18.44%	14.13%	10.71%	9.05%
	12	56.77%	28.53%	18.45%	14.13%	10.72%	9.06%
	16	57.28%	29.12%	18.93%	14.44%	10.93%	9.24%
	20	56.42%	28.14%	18.14%	13.93%	10.57%	8.93%
T1	0	56.89%	28.67%	18.56%	14.21%	10.77%	9.10%
	4	59.91%	32.34%	21.56%	16.15%	12.12%	10.27%
	8	63.50%	37.20%	25.74%	18.85%	14.00%	11.91%
	12	62.30%	35.52%	24.26%	17.90%	13.33%	11.33%
	16	55.98%	27.64%	17.74%	13.67%	10.40%	8.78%
	20	57.67%	29.57%	19.29%	14.68%	11.10%	9.38%

At tumor location N1, the probability of failure is very sensitive to the existence of tumor lesion that a 4mm's tumor lesion can raise the probability by 25.87% for underweight cohort, 52.88% for normal weight cohort, 61.16% for overweight cohort, 47.22% for mild obesity cohort, 41.15% for moderate obesity cohort and 37.78% for extreme obesity cohort. For the bones with even larger tumors, failure probability stabilizes and stays in a very high level for the first 3 BMI cohorts, while the 3 obesity cohorts had a continuous rise of the probability which eventually reaches around 90%.

At location N2, the influence of tumor lesion is very similar to that in location N1 but in a miner level with respect of probability of failure. However, when the lesion size reaches 20mm, the stress concentration factor for N2 is even greater than that of N1 with the highest probability of failure. The lesion at location N3 does not have a significant influence on probability of failure when the size of tumor lesion is small. However, the probability of failure had a major boost when the size reaches 20mm. At location H1, the probability of failure barely had any change among different lesion sizes. For location T1, the tumor does not have a significant influence on probability of failure. However, the highest probability of failure appeared at the size of 8mm instead of 20mm.

Regions like superior side and anterior side of femoral neck are very sensitive to tumor lesions in terms of probability of failure no matter what size it is. Even the high BMI cohorts receive considerable influence from the tumor lesion and have great chance of fracture when the lesion is large enough. Any tumor lesion found in this region requires attentions and clinical precautions such as protective padding and walk assistance. The inferior side of femoral neck usually has thicker cortex shell and allows small lesions on it without significant raise on the probability of failure in a sideways fall. Similarly,

tumor lesion on the superior side of femoral head has negligible influence in probability of failure of a sideways fall.

CHAPTER 8

DISCUSSION AND FUTURE WORK

The purpose of this study is to employ the probabilistic approach in evaluation and validation of the BMI influence in a sideways fall for a postmenopausal women cohort and examine the tumor lesions' influence under the same situation.

On the contrary with the deterministic approach such as factor of risk which is defined as the ratio between estimated hip fall force and failure strength, the probabilistic margin of safety approach is able to quantify the failure probability that reflect the stochastic nature of bone fracture assessment by accounting for the probability density functions of various random factors.

From an experiment approach, we explored and verified that BMI is a strong and comprehensive factor determining important aspects of sideways falls including BMD (bone mineral density), femur geometry, peak fall force, maximum von Mises stress and probability of hip fracture. The application of margin of safety method provides insight of hip fracture and is building the bridge between the FEA/in vitro experiments and large health investigation results.

There are also several limitations in this study. Due to lack of direct observation to our target cohort, we assumed the bone material to be homogeneous and isotropic, ignoring the longitudinal and transverse anisotropy and variation of BMD within proximal femur. The current QCT scan measures the volumetric BMD but is usually performed on bone samples due to radiation problem to patients. Anisotropy of bone material requires more information about the inner structures of trabeculae rather than Hounsfield numbers only.

The calculation is based on a passive sideways fall with a certain impact on the femur, indicating there is no mitigation of the fall by actions of the individual. Thus, we expect our predicted probability of failure to be substantially higher than actual hip fracture rates with respect to the total reported falls. Since there is no such statistics data on post fall behaviors of the target cohort, it is difficult to conclude the actual number of falls that end up with impacts on the hip region so that we can only compare the normalized incident rate of hip fracture.

The idealization and parameterization of tumor lesions ignore the influence from the tumor morphology which might have certain influence on the stress concentration effect. With more test data such as QCT scan to a specific tumor damaged femur case and medical records like detailed post fall observations to a cohort, the model would be better in predicting probability of hip fractures under certain conditions.

REFERENCES

a Fall, What Can Happen After. Important facts about falls. AAOS.org. *Bone tumor*. Retrieved 6/23, 2017, from http://orthoinfo.aaos.org/topic.cfm?topic=a00074

Abdelhafiz, A. H., & Austin, C. A. (2003). Visual factors should be assessed in older people presenting with falls or hip fracture. *Age and Ageing, 32*(1), 26-30.

Amin, S., Kopperdhal, D. L., Melton, L. J., Achenbach, S. J., Therneau, T. M., Riggs, B. L., et al. (2011). Association of hip strength estimates by finite-element analysis with fractures in women and men. *Journal of Bone and Mineral Research, 26*(7), 1593-1600.

Beck, T. J., Petit, M. A., Wu, G., LeBoff, M. S., Cauley, J. A., & Chen, Z. (2009). Does obesity really make the femur stronger? BMD, geometry, and fracture incidence in the women's health Initiative-Observational study. *Journal of Bone and Mineral Research, 24*(8), 1369-1379.

Bouxsein, M. L., Szulc, P., Munoz, F., Thrall, E., Sornay-Rendu, E., & Delmas, P. D. (2007). Contribution of trochanteric soft tissues to fall force estimates, the factor of risk, and prediction of hip fracture risk. *Journal of Bone and Mineral Research, 22*(6), 825-831.

Carballido-Gamio, J., Bonaretti, S., Saeed, I., Harnish, R., Recker, R., Burghardt, A. J., et al. (2015). Automatic multi-parametric quantification of the proximal femur with quantitative computed tomography. *Quantitative Imaging in Medicine and Surgery, 5*(4), 552.

Cauley, J. A., Blackwell, T., Zmuda, J. M., Fullman, R. L., Ensrud, K. E., Stone, K. L., et al. (2010). Correlates of trabecular and cortical volumetric bone mineral density at the femoral neck and lumbar spine: The osteoporotic fractures in men study (MrOS). *Journal of Bone and Mineral Research, 25*(9), 1958-1971.

Cummings, S. R., Nevitt, M. C., Browner, W. S., Stone, K., Fox, K. M., Ensrud, K. E., et al. (1995). Risk factors for hip fracture in white women. *New England Journal of Medicine, 332*(12), 767-774.

Dieter, G. E., & Schmidt, L. C. (2013). *Engineering design* McGraw-Hill New York.

Dragomir-Daescu, D., Den Buijs, J. O., McEligot, S., Dai, Y., Entwistle, R. C., Salas, C., et al. (2011). Robust QCT/FEA models of proximal femur stiffness and fracture load during a sideways fall on the hip. *Annals of Biomedical Engineering, 39*(2), 742-755.

Dufour, A. B., Roberts, B., Broe, K. E., Kiel, D. P., Bouxsein, M. L., & Hannan, M. T. (2012). The factor-of-risk biomechanical approach predicts hip fracture in men and women: The framingham study. *Osteoporosis International, 23*(2), 513-520.

Easley, S. K., Pal, S., Tomaszewski, P. R., Petrella, A. J., Rullkoetter, P. J., & Laz, P. J. (2007). Finite element-based probabilistic analysis tool for orthopaedic applications. *Computer Methods and Programs in Biomedicine, 85*(1), 32-40.

Felippa, C. (2004). *Introduction to Finite Element Methods (ASEN 5007)-Fall 2004 Department of Aerospace Engineering Sciences, University of Colorado at Boulder*,

Felson, D. T., Anderson, J. J., Hannan, M. T., Milton, R. C., Wilson, P. W., & Kiel, D. P. (1989). Impaired vision and hip fracture. *Journal of the American Geriatrics Society, 37*(6), 495-500.

Greenspan, S. L., Myers, E. R., Maitland, L. A., Resnick, N. M., & Hayes, W. C. (1994). Fall severity and bone mineral density as risk factors for hip fracture in ambulatory elderly. *Jama, 271*(2), 128-133.

Grisso, J. A., Kelsey, J. L., Strom, B. L., Ghiu, G. Y., Maislin, G., O'brien, L. A., et al. (1991). Risk factors for falls as a cause of hip fracture in women. *New England Journal of Medicine, 324*(19), 1326-1331.

Hayes, W., & McMahon, T. (1991). Prediction of femoral impact forces in falls on the hip. *Age, 24*, 30.

Hayes, W. C., Myers, E. R., Morris, J. N., Gerhart, T. N., Yett, H. S., & Lipsitz, L. A. (1993). Impact near the hip dominates fracture risk in elderly nursing home residents who fall. *Calcified Tissue International, 52*(3), 192-198.

Laing, A. C., Tootoonchi, I., Hulme, P. A., & Robinovitch, S. N. (2006). Effect of compliant flooring on impact force during falls on the hip. *Journal of Orthopaedic Research, 24*(7), 1405-1411.

Magaziner, J., Hawkes, W., Hebel, J. R., Zimmerman, S. I., Fox, K. M., Dolan, M., et al. (2000). Recovery from hip fracture in eight areas of function. *The Journals of Gerontology.Series A, Biological Sciences and Medical Sciences, 55*(9), M498-507.

Maitland, L. A., Myers, E. R., Hipp, J. A., Hayes, W. C., & Greenspan, S. L. (1993). Read my hips: Measuring trochanteric soft tissue thickness. *Calcified Tissue International, 52*(2), 85-89.

Mayhew, P. M., Thomas, C. D., Clement, J. G., Loveridge, N., Beck, T. J., Bonfield, W., et al. (2005). Relation between age, femoral neck cortical stability, and hip fracture risk. *The Lancet, 366*(9480), 129-135.

Morgan, E. F., Bayraktar, H. H., & Keaveny, T. M. (2003). Trabecular bone modulus–density relationships depend on anatomic site. *Journal of Biomechanics, 36*(7), 897-904.

Nielson, C. M., Marshall, L. M., Adams, A. L., LeBlanc, E. S., Cawthon, P. M., Ensrud, K., et al. (2011). BMI and fracture risk in older men: The osteoporotic fractures in men study (MrOS). *Journal of Bone and Mineral Research, 26*(3), 496-502.

Nishiyama, K. K., Gilchrist, S., Guy, P., Cripton, P., & Boyd, S. K. (2013). Proximal femur bone strength estimated by a computationally fast finite element analysis in a sideways fall configuration. *Journal of Biomechanics, 46*(7), 1231-1236.

Orwoll, E. S., Marshall, L. M., Nielson, C. M., Cummings, S. R., Lapidus, J., Cauley, J. A., et al. (2009). Finite element analysis of the proximal femur and hip fracture risk in older men. *Journal of Bone and Mineral Research, 24*(3), 475-483.

pathorama.ch. (2017). Telangiectatic osteosarcoma. Retrieved 6/23, 2017, from http://www.webpathology.com/image.asp?n=59&Case=335

Ray, W. A., Griffin, M. R., Schaffner, W., Baugh, D. K., & Melton III, L. J. (1987). Psychotropic drug use and the risk of hip fracture. *New England Journal of Medicine, 316*(7), 363-369.

Robinovitch, S. N., McMahon, T. A., & Hayes, W. C. (1995). Force attenuation in trochanteric soft tissues during impact from a fall. *Journal of Orthopaedic Research, 13*(6), 956-962.

Snyder, B. D., Hauser-Kara, D. A., Hipp, J. A., Zurakowski, D., Hecht, A. C., & Gebhardt, M. C. (2006). Predicting fracture through benign skeletal lesions with quantitative computed tomography. *The Journal of Bone and Joint Surgery.American Volume, 88*(1), 55-70.

Turner, M., Clough, R., Martin, H., & Topp, L. (1956). Stiffness and deflection analysis of complex structures, J. of aero. *Sc, 23*, 174.

van den Kroonenberg, Aya J, Hayes, W. C., & McMahon, T. A. (1996). Hip impact velocities and body configurations for voluntary falls from standing height. *Journal of Biomechanics, 29*(6), 807-811.

Young, W. C., & Budynas, R. G. (2002). *Roark's formulas for stress and strain* McGraw-Hill New York.

Zienkiewicz, O. C., Taylor, R. L., Zienkiewicz, O. C., & Taylor, R. L. (1977). *The finite element method* McGraw-hill London.

Zysset, P., Pahr, D., Engelke, K., Genant, H. K., McClung, M. R., Kendler, D. L., et al. (2015). Comparison of proximal femur and vertebral body strength improvements in the FREEDOM trial using an alternative finite element methodology. *Bone, 81*, 122-130.